HIGH-RESOLUTION ROTATION CURVES OF LOW SURFACE BRIGHTNESS GALAXIES. II. MASS MODELS

W. J. G. DE BLOK[1]

Australia Telescope National Facility, P.O. Box 76, Epping, NSW 1710, Australia; edeblok@atnf.csiro.au

STACY S. MCGAUGH

Department of Astronomy, University of Maryland, College Park, MD 20742-2421; ssm@astro.umd.edu

AND

VERA C. RUBIN

Department of Terrestrial Magnetism, Carnegie Institution of Washington, 5241 Broad Branch Road, N.W., Washington, DC 20015; rubin@dtm.ciw.edu

ABSTRACT

We present mass models for a sample of 30 high-resolution rotation curves of low surface brightness galaxies. We fit both pseudoisothermal (core dominated) and cold dark matter (CDM; cusp dominated) halos for a wide variety of assumptions about the stellar mass-to-light ratio. We find that the pseudoisothermal model provides superior fits. CDM fits show systematic deviations from the data and often have a small statistical likelihood of being the appropriate model. The distribution of concentration parameters is too broad, and has too low a mean, to be explained by low-density, flat CDM (ΛCDM). This failing becomes more severe as increasing allowance is made for stellar mass: Navarro, Frenk, & White (NFW) model fits require uncomfortably low mass-to-light ratios. In contrast, the maximum disk procedure does often succeed in predicting the inner shape of the rotation curves, but it requires uncomfortably large stellar mass-to-light ratios. The data do admit reasonable stellar population mass-to-light ratios if halos have cores rather than cusps.

Key words: dark matter — galaxies: fundamental parameters — galaxies: kinematics and dynamics

On-line material: machine-readable table

1. INTRODUCTION

1.1. *LSB Galaxies*

Over the last 5 years, the rotation curves of low surface brightness (LSB) galaxies and the constraints they impose on cosmological theories have received much attention in the literature. An LSB galaxy is usually defined as a disk galaxy with an extrapolated central disk surface brightness $\gtrsim 1$ mag arcsec^{-2} fainter than the typical value for "normal" high surface brightness (HSB) spiral galaxies (Freeman 1970). Colors, metallicities, gas fractions, and extensive population synthesis modeling all support the idea that LSB galaxies are unevolved galaxies with low (current and past) star formation rates (e.g., van der Hulst et al. 1993; McGaugh & Bothun 1994; McGaugh 1994; McGaugh & de Blok 1997; de Blok, van der Hulst, & Bothun 1995; van den Hoek et al. 2000; Bell et al. 2000; see Bothun, Impey, & McGaugh 1997 for a review).

The observation that LSB and HSB galaxies follow the same Tully-Fisher (T-F) relation requires (in the conventional picture) that LSB galaxies are dominated by dark matter (Zwaan et al. 1995; Sprayberry et al. 1995; Verheijen 1997; de Blok & McGaugh 1996). For reasonable stellar mass-to-light ratios Υ_*, low surface brightness implies low stellar density. Yet the extended, low surface density stellar disks cannot be the major contributors to the dynamics in LSB galaxies, as no shift in the zero point of the T-F relation with surface brightness is observed. This contrasts with the dominance of the stellar population in HSB galaxies of similar luminosity.

The modest Υ_*-values, as implied by the blue colors and the (baryonic) T-F relation, together with the diffuseness of the stellar disks, make analyses of the dark matter distribution in LSB galaxies less ambiguous than in HSB galaxies, where the stellar component can be significant even for fairly low Υ_*-values. LSB galaxies are therefore ideal laboratories for measuring the distribution of dark matter for comparison with predictions of theories of galaxy formation.

For example, one of the results of numerical cold dark matter (CDM) simulations is a so-called universal halo mass-density profile (Navarro, Frenk, & White 1996), commonly known as an "NFW profile." NFW (and all CDM) mass-density profiles are characterized by steep central cusps. This is in contrast with the other commonly used "classic" pseudoisothermal sphere halo model, which is characterized by a constant-density core. The parameters of the NFW mass-density distribution are related to the mass of the halo and the density of the universe at the time of collapse and are therefore set by the cosmology. As these parameters can be determined from observations, this opens the possibility of testing the NFW CDM model, as well as its underlying assumptions.

A first analysis of LSB galaxy H I rotation curves by de Blok & McGaugh (1997) indicated that they did not rise as steeply as their HSB counterparts of similar luminosity, contrary to CDM predictions. The mass distribution in LSB galaxies is more extended and of lower density than in HSB galaxies (de Blok & McGaugh 1996).

Other results also indicate that the steep rotation curves implied by CDM are hard to reconcile with the observed shallow rotation curves of dwarf galaxies (Moore 1994; Flores & Primack 1994; Blais-Ouellette, Amram, & Carig-

---
[1] Bolton Fellow.

nan 2001; Côté, Carignan, & Freeman 2000; Salucci 2001). To explain this discrepancy, the possibility of redistribution of the (cuspy) dark matter due to violent star formation (thus creating the observed cores) was sometimes raised, but this has been shown to be inconsistent with other observational data (Mac Low & Ferrara 1999).

McGaugh & de Blok (1998) argued that the shapes of rotation curves of LSB galaxies were inconsistent with those predicted by the NFW prescription. This could not be explained by the effects of star formation, as the larger masses of LSB galaxies would require large bursts in order to redistribute matter on large scales. Their quiescent evolutionary history argues strongly against this (van den Hoek et al. 2000).

This comparison with the CDM model is often dismissed because of the limited resolution of the observed H I curves. The early H I LSB rotation curves were obtained using the VLA and the Westerbork Synthesis Radio Telescope. The relatively large beams of these instruments resulted in rotation curves with only limited resolution. De Blok & McGaugh (1997) did however show that for the best-resolved cases, the effects of beam smearing were not strong enough to explain the observed shallow curve as being simply the result of a steep NFW model curve affected by beam smearing. Similar results were found for more fashionable cosmologies, such as ΛCDM ($\Omega_m \sim 0.3$, $\Omega_\Lambda \sim 0.7$), though with smaller discrepancies.

Even so, the theoretical debate now seems to have settled on halos with cusps even steeper than NFW halos (Moore et al. 1999), thus worsening the possible conflict between the data and the simulations. From the observational point of view, the easiest and least ambiguous way to test the reality of these discrepancies is to measure high-resolution rotation curves.

1.2. Optical Rotation Curves

Optical Hα rotation curves of five LSB galaxies from the sample of de Blok, McGaugh, & van der Hulst (1996, hereafter BMH) were presented by Swaters, Madore, & Trewhella (2000, hereafter SMT). Though SMT found that for two of the five galaxies the inner slopes of the rotation curves were steeper than derived from the H I observations, this difference does not affect the BMH conclusion that LSB rotation curves have shallower slopes than HSB rotation curves of similar amplitude. Because of these steeper slopes, SMT derive higher maximum disk Υ_*-values (in some cases over 10), strengthening one of the conclusions from de Blok & McGaugh (1997), that the maximum Υ_*-values in LSB galaxies are too large to be accommodated by reasonable star formation histories and initial mass functions. Such high values are inconsistent with the existence of a baryonic T-F relation (McGaugh et al. 2000).

A different approach was taken by van den Bosch et al. (2000). They attempted to apply a rigorous correction for beam smearing to the BMH H I data and thus to derive the true "infinite resolution" rotation curve. They conclude that the data are not of high enough resolution to accept or reject the NFW hypothesis with any significance. However, as they use a modified NFW profile with the inner slope of the mass-density distribution as an (additional) free parameter, it is not clear how significant this conclusion is. The usual three-parameter rotation-curve fits are already underconstrained; adding another parameter does not improve the significance of the results. Furthermore, in some cases

they find such low values for the inner slope that their NFW halos effectively become core dominated. These halos do of course fit the data, but they do not occur in CDM simulations.

The general picture as derived from early observations of rotation curves of LSB galaxies therefore still holds: LSB galaxies are unevolved, low-density galaxies, dominated by dark matter. Their rotation curves have shallower slopes than those of HSB galaxies of similar amplitude, and the shapes of the best-resolved LSB curves are not necessarily consistent with the NFW rotation-curve shapes.

1.3. New Data

In this paper, we present an analysis of high-resolution high-quality hybrid Hα/H I rotation curves of a sample of 30 LSB galaxies. Of this sample, 26 curves were taken from the large sample of 50 LSB galaxies presented in McGaugh, Rubin, & de Blok (2001, hereafter Paper I). In that paper, an extensive description is given of the data, the sample, and reduction method. We also refer to Paper I for a comparison of the new Hα data with the BMH H I curves. We also reanalyze the data for an additional five curves taken from SMT. In this paper, we derive mass models under various assumptions for Υ_* and fit these models with both NFW halos and pseudoisothermal halos. A similar analysis for a different set of rotation curves of dwarf and LSB galaxies is given in de Blok & Bosma (2001).

In § 2, we discuss the sample and discuss the derivation of the rotation curves. We also show internal and external comparisons of the data and discuss possible systematics. In § 3, we discuss the various mass models. Section 4 contains the results of the model fitting. Section 5 discusses the implications for the various halo models. In § 6 we turn our attention to the maximum disk, and a summary is given in § 7. When using absolute distances, we have used a Hubble constant $H_0 = 75$ km s^{-1} Mpc^{-1}.

2. THE DATA

2.1. Sample and Raw Data

The data and reduction methods are extensively described in Paper I. In summary, we use long-slit majoraxis spectra taken with the 4 m telescope at Kitt Peak in 1999 June and 2000 February and the 100 inch (2.5 m) telescope at Las Campanas in 1998 November. Velocities were derived from the intensity-weighted centroid of the Hα and [N II] lines.

As the aim of this exercise is to derive mass models that can yield significant constraints on the distribution of dark matter, we select only the 26 high-quality galaxies from Paper I. We split this high-quality sample into two subsamples. Sample I contains LSB galaxies from BMH and van der Hulst et al. (1993) for which a full set of photometry and H I data is available. In sample I, we also include the five galaxies presented by SMT. For these galaxies H I and optical photometry are taken from BMH. Tables 1 and 2 contain a full list of the galaxies analyzed here, along with some of their global parameters.

Sample II consists of ESO-LV and UGC LSB galaxies, for which an optical rotation curve is available but no optical or H I photometry.

For the galaxies in sample I, H I observations are available that often extend to larger radii than the Hα data. To make the best use of both types of data, we have con-

TABLE 1

SAMPLE I: GALAXIES WITH PHOTOMETRY

Name (1)	D (Mpc) (2)	$\mu_0(B)$ (mag arcsec^{-2}) (3)	h (kpc) (4)	$M_{abs}(B)$ (mag) (5)	R_{max} (kpc) (6)	V_{max} (km s^{-1}) (7)	V_{hel} (km s^{-1}) (8)	i (deg) (9)
F563-1	45	23.6	2.8	-17.3	17.7	112	3502	25
F563-V2	61	22.1	2.1	-18.2	9.2	118	4312	29
F568-1	85	23.8	5.3	-18.1	14.9	142	6524	26
F568-3	77	23.1	4.0	-18.3	16.5	105	5913	40
F568-V1	80	23.3	3.2	-17.9	19.0	118	5768	40
F571-8	48	23.9[a]	5.2	-17.6[a]	15.6	144	3768	90
F574-1	96	23.3[a]	4.3	-18.4[a]	15.4	100	6889	65
F579-V1	85	22.8[a]	5.1	-18.8[a]	17.3	114	6305	26
F583-1	32	24.1	1.6	-16.5	14.6	87	2264	63
F583-4	49	23.8[a]	2.7	-16.9[a]	10.0	70	3617	55
UGC 5750......	56	23.5[a]	5.6	-18.7[a]	21.8	79	4177	64
UGC 6614......	85	23.4	8.1	-20.3	62	204	6371	36

NOTE.—Col. (2): Distance computed assuming Hubble flow after correction for Galactic rotation and Virgocentric flow. Col. (6): Maximum radius of rotation curve. Col. (7): Maximum velocity in rotation curve. Col. (8): Heliocentric systemic velocity. Photometric and distance data are from de Blok & McGaugh 1997; R_{max}, V_{max}, and V_{sys} are derived from new optical curves.

[a] Converted from R band assuming $B - R = 0.9$.

structed hybrid rotation curves. These consist of the Hα data over the range of radii where available, and 21 cm data to define the outermost points. No attempt has been made to "average" the different types of data: Hα is given precedence over the range of radii where it is available.

2.2. Derivation of the Smooth Curves

One of the main assumptions made when deriving mass models from rotation curves is that the gas and stars trace circular orbits in an axisymmetric potential. Though the shape of the optical rotation curves in Paper I is well defined, the scatter between individual data points means

we cannot simply use the raw rotation curves to estimate the radial run of the gravitational potential. For this, one needs a smooth curve that retains real small-scale details, but without the observational scatter.

The method most often used to produce these smooth curves is to fit splines to the data. Here we have used a robust version of this procedure (local regression; see Loader 1999). The smooth curves were rebinned to a bin width of 2″. The error bars in the rebinned data points consist of two components: one due to observational errors caused by the measurement uncertainties in the individual raw data points (for this we use the average weighted mea-

TABLE 2

SAMPLE II: GALAXIES WITHOUT PHOTOMETRY

Name (1)	D (Mpc) (2)	V_{hel} (km s^{-1}) (3)	$M_{abs}(B)$ (mag) (4)	R_{max} (kpc) (5)	V_{max} (km s^{-1}) (6)	i (deg) (7)
F730-V1	144	10714	...	11.9	145	50
UGC 4115	3.2	343	-12.4	1.0	40	74
UGC 11454	91	6628	-18.6[a]	11.9	152	64
UGC 11557	22	1390	-20.0	6.2	95	36
UGC 11583	5	128	-14.0[a]	1.5	36	83
UGC 11616	73	5244	-20.3[a]	9.6	143	60
UGC 11648	48	3350	-21.0[a]	12.7	145	90
UGC 11748	73	5265	-22.9[a]	21.0	242	78
UGC 11819	60	4261	-20.3[a]	11.7	153	66
ESO-LV 014-0040......	212	16064	-21.6	29.2	263	35
ESO-LV 084-0411......	80	6200	-18.1	8.9	61	90
ESO-LV 120-0211......	15	1314	-15.6	3.5	25	70
ESO-LV 187-0510......	18	1410	-16.5	3.0	40	58
ESO-LV 206-0140......	60	4704	-19.2	11.6	118	39
ESO-LV 302-0120......	69	5311	-19.1	11.0	86	55
ESO-LV 305-0090......	11	1019	-17.3	4.8	54	53
ESO-LV 425-0180......	86	6637	-20.5	14.4	145	33
ESO-LV 488-0490......	22	1800	-16.8	6.0	97	63

NOTE.—Cols. (2) and (3): Distance D was calculated from V_{hel} after correcting for Galactic rotation and assuming pure Hubble flow with $H_0 = 75$ km s^{-1} Mpc^{-1}. Col. (4): Absolute magnitude computed using apparent magnitudes from the ESO-LV catalog and the RC3 and corrected for foreground Galactic extinction.

[a] The apparent magnitude is Zwicky magnitude 17 and therefore very uncertain.

surement error in each bin), and an additional component caused by differences between approaching and receding sides and noncircular motions (which we define as the difference between the weighted mean raw velocity and the velocity implied by the spline fit at that radius). For the final error estimate, these two uncertainties were added quadratically.

For some high signal-to-noise data points, the error bars become unrealistically small (sometimes less than 1 km s^{-1}). This has no physical significance and simply tells us that the profile centroids were well determined. These small error bars can, however, easily dominate any model fit and can severely bias χ^2 values or goodness-of-fit parameters. For this reason, and as the observational and physical uncertainties (slit position, streaming motions) make it difficult to determine a physically meaningful rotation velocity with an accuracy of more than a few kilometers per second, we have imposed a minimum error on each point of 4 km s^{-1} (before inclination correction). The curves were corrected for inclination using the values given in Tables 1 and 2.

The end result is a smooth representation of the data, which is reproducible and as objective as possible, to use as input for the mass models. Figure 1 shows overlays of both the raw hybrid curves and the smooth versions. It is easy to verify that no systematic differences in slope or shape have been introduced. The error bars in the smooth curves are also a good representation of the uncertainties in the underlying raw data.

Table 3 contains the hybrid smooth rotation curves. For each galaxy we list the radii in arcseconds, as well as in kiloparsecs, together with the observed rotation velocities and the uncertainties in these values. Also included are the rotation curves for the gas component (already included is the factor of 1.4 mass scaling for He), the disk component [values listed assume $\Upsilon_*(R) = 1.0$], and where applicable the bulge component [also for $\Upsilon_*(R) = 1.0$].

2.3. Comparing the Smooth Curves

As noted above, we have included the five LSB galaxies presented by SMT in our sample I. As SMT show their raw data and derived smooth curves, we can compare both sets of smooth rotation curves to investigate possible systematics in our respective methods. This is done in Figure 2. It is clear that the correspondence between both velocities and error bars is good and the differences are minor. In most cases (F568-1, F568-V1, and F574-1) both sets agree at
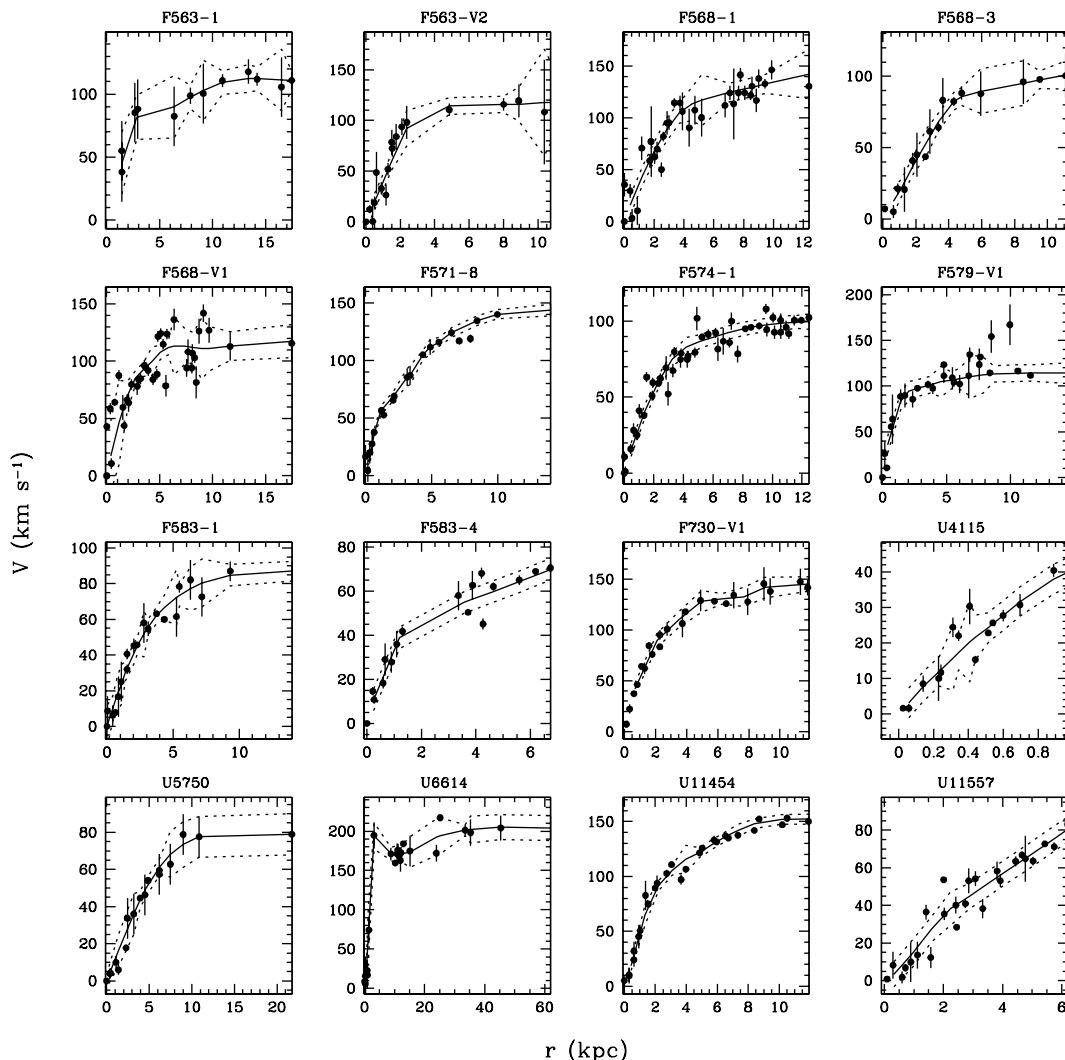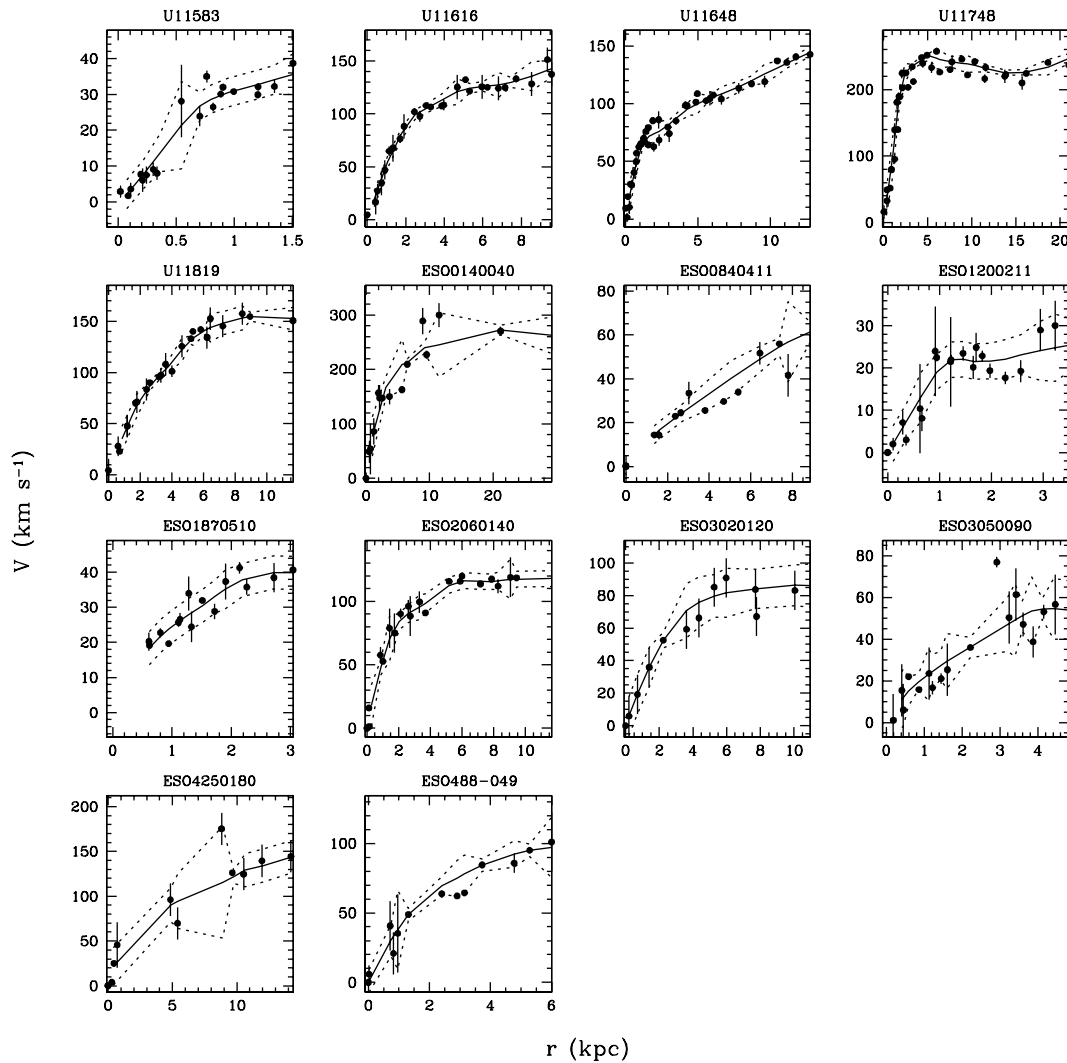

FIG. 1.—Comparison of the raw hybrid rotation curves (circles) with the smooth curves (solid lines). The derived uncertainties in the smooth curves are indicated by the dotted lines.

Fig. 1.—Continued

(better than) the 1 σ level. Small remaining differences are usually caused by a slightly different estimate of the velocities in sparsely sampled parts (F563-V2 and F568-3). The SMT curve for F563-V2 (Fig. 2, *top left*) is slightly higher than our curve in the inner parts but falls below ours in the outer parts. The sparseness of optical data points in the outer parts and different interpretations of the continuity

between H I and optical data are probably the main cause of this difference. For F568-3 (Fig. 2, *bottom*), we find a small ($\lesssim 1$ σ) systematic difference between both smooth curves. This galaxy has been measured independently by SMT and by us (Paper I). These raw data sets agree in detail, and the difference must therefore be due to a slightly different interpretation of the sparse raw data. In summary,

TABLE 3
MODELED ROTATION CURVES

R (arcsec)	R (kpc)	V_{gas}[a,b] (km s^{-1})	V_{disk}[a,c] (km s^{-1})	V_{bulge}[a,c] (km s^{-1})	V_{obs} (km s^{-1})	σ_V (km s^{-1})
F583-1:						
0.3......	0.1	−0.1	0.4	0	1.1	11.1
2.8......	0.4	−0.9	4.0	0	10.0	7.0
5.0......	0.7	−1.5	6.7	0	17.4	9.6
6.9......	1.0	−2.2	8.5	0	23.5	11.2
9.0......	1.4	−2.8	10.1	0	31.0	5.2

NOTE.—Table 3 is presented in its entirety in the electronic edition of the Astronomical Journal. A portion is shown here for guidance regarding its form and content.
[a] Only given when known (sample I). Set to zero if unknown.
[b] Assumes $M_{gas} = 1.4 M_{HI}$.
[c] For $M/L = 1.0$ in the R band.
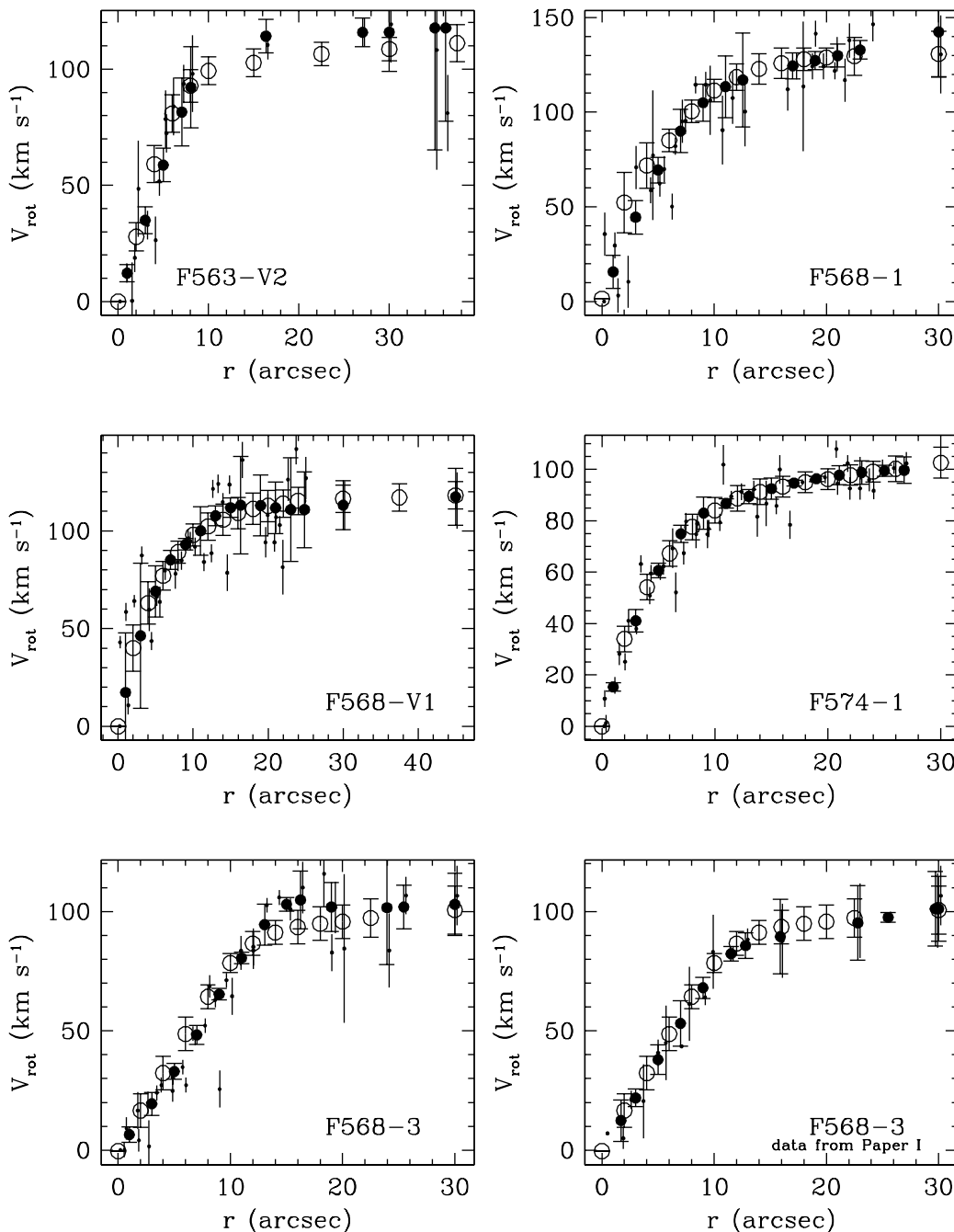
FIG. 2.—Comparison of our analysis of the SMT data with their resampled rotation curves. The top four panels and the bottom left panel show the raw data from SMT (*dots*), their resampled and smoothed rotation curves (*open circles*), and our local regression fits to the same data (*filled circles*). The raw data have been offset by +0″.2 to avoid overlap with the binned data. The bottom right panel shows the raw data for F568-3 taken from Paper I, along with the SMT model (identical to the model shown in the bottom left panel) and our resampled rotation curve based on the data from Paper I. Small differences between the various curves are discussed in the text.

the smooth curves we present here give a good and reproducible representation of the data.

3. MASS MODELS

In order to find the signature of the dark halo, one needs to model the observed rotation curve using a number of separate dynamical components, described below.

3.1. *Stellar Component*

To model the stellar disk, the *R*-band photometry presented in de Blok et al. (1995) was used. The rotation curve of the disk was computed following Casertano (1993) and

Begeman (1987). The disk was assumed to have a vertical $sech^2$ distribution with a scale height $z_0 = h/6$ (van der Kruit & Searle 1981). The rotation curves of the stellar component were resampled at the same radii as the smooth curves. We assume that Υ_* is constant with radius. While one expects some modest variation in Υ_* with radius (de Jong 1996), the color gradients in LSB galaxies tend to be small, so this effect is not likely to be significant.

3.2. *Gas Disk*

The H I surface density profiles presented in BMH and van der Hulst et al. (1993) were used. They were scaled by a

factor of 1.4 to take the contribution of helium and metals into account. Their rotation curve was derived assuming the gas was distributed in a thin disk. The gas rotation curves were resampled at the radii of the smooth observed rotation curve.

3.3. Dark Halo

The dark halo component differs from the previous two in that we are interested in parameterizing this component assuming some fiducial model. The choice of this model is the crux of most of the dark matter analyses in the literature, and many models exist. These can be broadly distinguished in two groups: halo models with a core, and halo models with a cusp. An example of the first category is the pseudoisothermal halo; an example of the latter, the CDM NFW halo.

As one of the goals of this paper is to assess the relevance of either category to the high-resolution LSB galaxy rotation curves, we will present models derived using both models. We do realize that there are many intermediate models described in the literature that probably can fit our data equally well. However, our goal here is simply to see where the data lead us: is there a preference for models with a core or with a cusp? We now describe the details of both models.

3.3.1. Pseudoisothermal Halo

The spherical pseudoisothermal halo has a density profile

$$\rho_{\rm iso}(R) = \rho_0[1 + (R/R_C)^2]^{-1} , \qquad (1)$$

where ρ_0 is the central density of the halo and R_C is the core radius of the halo. The corresponding rotation curve is given by

$$V(R) = \sqrt{4\pi G\rho_0 R_C^2\left[1 - \frac{R_C}{R}\arctan\left(\frac{R}{R_C}\right)\right]} . \qquad (2)$$

The asymptotic velocity of the halo, V_∞, is given by

$$V_\infty = \sqrt{4\pi G\rho_0 R_C^2} . \qquad (3)$$

To characterize this halo only two of the three parameters (ρ_0, R_C, V_∞) are needed, as equation (3) determines the value of the third parameter.

3.3.2. NFW Halo

The NFW mass-density distribution takes the form

$$\rho_{\rm NFW}(R) = \frac{\rho_i}{(R/R_s)(1 + R/R_s)^2} , \qquad (4)$$

where R_s is the characteristic radius of the halo and ρ_i is related to the density of the universe at the time of collapse. This mass distribution gives rise to a halo rotation curve

$$V(R) = V_{200}\sqrt{\frac{\ln(1 + cx) - cx/(1 + cx)}{x[\ln(1 + c) - c/(1 + c)]}} , \qquad (5)$$

where $x = R/R_{200}$. It is characterized by a concentration parameter $c = R_{200}/R_s$ and a radius R_{200}. These are directly related to R_s and ρ_i but are used instead, as they are a convenient way to parameterize the rotation curve. The radius R_{200} is the radius where the density contrast exceeds 200, roughly the virial radius (Navarro et al. 1996). The characteristic velocity V_{200} of the halo is defined in the same way as R_{200}. These parameters are not independent and are set by the cosmology.

3.4. Mass-to-Light Ratios and Weighting

One of largest uncertainties in any mass model is the value of Υ_*. Though broad trends in Υ_* have been measured and modeled (e.g., Bottema 1997; Bell & de Jong 2000), the precise value for an individual galaxy is not well known and depends on extinction, star formation history, initial mass function, etc. Rotation-curve fitting is a problem with too many free parameters (van Albada & Sancisi 1986; Lake & Feinswog 1989), and some assumptions regarding Υ_* must be made. We therefore present disk-halo decompositions using four different assumptions for Υ_* for the galaxies in sample I. For the galaxies in sample II, only the minimum disk model is presented.

Minimum disk.—This model assumes that the observed rotation curve is due entirely to dark matter. This gives an upper limit on how concentrated the dark mass component can actually be and is the version of minimum disk preferred in the CDM literature.

Minimum disk plus gas.—The contribution of the atomic gas (H I and He) is taken into account, but Υ_* is assumed to be zero. This is the classical definition of minimum disk as used in the H I rotation-curve literature.

Constant Υ_*.—Here Υ_* is set equal to a constant value based on an initial mass function (IMF) and a star formation history appropriate for LSB galaxies. For the range in color $0.4 < B - V < 0.65$ that LSB galaxies normally exhibit (de Blok et al. 1995), a value $\Upsilon_*(R) = 1.4$ is a good estimate. For example, using the Bruzual & Charlot (1993) model with constant star formation rate and Salpeter IMF, we find that $\Upsilon_*(R) = 1.4$ corresponds to $B - V = 0.46$. The PEGASE2 model (B. Rocca-Volmerange 2000, private communication) gives a value $B - V = 0.38$, whereas the model by Cole et al. (2000) yields $B - V = 0.67$. The models by Bell & de Jong (2001) give values around $B - V \simeq 0.6$. The value $\Upsilon_* = 1.4$ is thus actually at the "lightweight" end of the plausible range, but this was deliberately chosen in order to give maximum opportunity for the cuspy NFW models to fit the data. We realize that the values derived here should not be regarded as definitive: changes in the IMF model used or different estimates for internal extinction can lead to different values. However, here we attempt to derive a conservative estimate for Υ_* based on the observed properties of the stellar population. Further (upward) refinement of the Υ_*-value is thus more likely to cause more problems for NFW fits.

Maximum disk.—The rotation curve of the stellar component is scaled to the maximum value allowed by the (smooth) rotation curve, but with the restriction that the dark matter density is required to be positive at all radii (thus avoiding a so-called hollow halo) (van Albada & Sancisi 1986). Because of the different dark matter distributions that we test (core and cusp), this can occasionally lead to maximum disk values that differ slightly for each of the two models. A more extensive description is given in § 6.

Each of the rotation curves was fitted using the GIPSY task ROTMAS. The program determines the best-fitting combination of R_C and V_∞ (for the pseudoisothermal halo) or c and V_{200} (for the NFW halo), using a least-squares fitting routine. We assigned weights to the data points inversely proportional to the square of their uncertainty. Additional checks were made with other fitting programs to check the results of the fits (discussed in § 4.1 below). We also refitted the smooth rotation curves presented by SMT

and were able to reproduce the numbers given in their Table 2.

4. RESULTS

Tables 4 and 5 give the results of the model fitting using the NFW halo model. Tables 6 and 7 show the results for the pseudoisothermal halo. Figure 3 presents the results of the NFW halo and pseudoisothermal halo mass modeling for each galaxy, side by side. The two leftmost columns show the results for NFW halo fitting. The two rightmost columns show the pseudoisothermal halo fitting results.

The first and third columns in Figure 3 show the best-fitting models. The rotation curves of the gas are shown as dotted lines, those of the stellar disk component as short-dashed lines. In two cases (UGC 6614 and F571-8) a significant bulge was present, which was modeled separately; this is shown as the dot-dashed line (see also § 4.3). The resulting halo rotation curve is shown as the long-dashed line. The final total model curve is drawn as the solid line. In each of the model panels we also give the reduced χ^2 of the fit and the chance p that the data and the model could result from

the same parent distribution. This probability was derived using a simple χ^2 test; it is an indicator for the compatibility of the data and the model chosen to describe it. Values $p > 0.95$ indicate that the data and the model are a good match. Values $p < 0.05$ indicate that the model is incompatible with the data, and that better models can be found.

We show two best-fitting values: one as found by the linear fit of the GIPSY ROTMAS task (*plus sign*), and one found by finding the minimum in the plotted logarithmic parameter space (*cross*). These two are identical except when extreme parameter values occur (usually during maximum disk fits) and numerical precision of the fitting routine starts to play a role. This effect is visible in the bottom right corners of the NFW contour plots, where the very large values of V_{200} in combination with the small values of c cause increasingly ragged contours. A large difference between these two best values therefore indicates that the fit should not be regarded as definitive. Indeed, in a number of these cases (indicated in the tables by italic numbers) the fitting routine was unable to determine a valid solution, and an indicative value had to be chosen by hand.

TABLE 4
FITTING PARAMETERS: NFW HALO, SAMPLE I

GALAXY	MINIMUM DISK						MINIMUM DISK PLUS GAS					
	c	Δc	V_{200}	ΔV	χ^2_{red}	p	c	Δc	V_{200}	ΔV	χ^2_{red}	p
F563-1	10.7	1.2	93.1	4.3	0.092	0.999	11.3	1.3	87.5	3.9	0.089	0.999
F568-3	3.2	3.7	214.6	233.9	2.239	0.017	4.2	3.3	161.3	118.9	2.386	0.011
F571-8	7.8	1.1	163.8	20.2	1.501	0.123	7.8	1.1	163.3	20.1	1.477	0.132
F579-V1	20.9	1.5	78.4	2.6	0.211	0.998	22.1	1.6	75.1	2.5	0.217	0.998
F583-1	5.1	1.0	106.6	17.0	0.740	0.746	6.2	1.1	86.6	12.4	0.827	0.648
F583-4	5.7	1.4	89.5	19.0	0.322	0.944	6.1	1.4	82.2	15.5	0.321	0.945
UGC 5750......	2.6	1.5	123.1	58.8	1.243	0.262	2.9	1.6	105.8	47.7	1.203	0.288
UGC 6614......	10.3	2.0	169.8	17.7	4.626	0.000	11.0	2.2	163.9	17.1	4.712	0.000
	SMT Data, Our Analysis											
F563-V2	7.5	3.7	153.1	70.5	1.391	0.195	8.3	3.8	133.1	54.1	1.484	0.157
F568-1	6.4	2.4	194.6	71.9	0.804	0.625	7.5	2.4	160.1	46.7	0.869	0.562
F568-3	*1.2*	...	*591.1*	...	3.551	0.000	*1.2*	...	552.6	...	3.573	0.000
F568-V1	14.6	1.2	92.0	4.9	0.197	0.999	15.7	1.5	87.2	5.0	0.242	0.997
F574-1	8.3	1.3	98.3	10.4	1.595	0.085	9.0	1.5	91.1	9.4	1.806	0.041

GALAXY	CONSTANT $\Upsilon_*(R) = 1.4$						MAXIMUM DISK						
	c	Δc	V_{200}	ΔV	χ^2_{red}	p	c	Δc	V_{200}	ΔV	χ^2_{red}	p	Υ_*^R
F563-1	9.9	1.2	88.8	4.6	0.089	0.999	4.0	1.2	110.0	20.1	0.098	0.999	6.9
F568-3	2.3	4.9	218.6	410.9	2.127	0.024	0.4	19.5	595.0	∞	2.015	0.024	2.2
F571-8	1.6	5.7	591.4	...	3.776	0.012	*1.0*	...	500.0	...	7.060	0.000	4.2
F579-V1	23.2	1.9	67.9	2.4	0.215	0.998	43.4	14.6	31.6	3.9	0.671	0.781	7.9
F583-1	5.4	1.1	90.6	14.7	0.767	0.716	2.2	1.5	145.5	78.7	0.680	0.804	6.5
F583-4	5.9	1.4	76.0	14.5	0.271	0.965	11.4	6.1	12.9	3.3	0.196	0.986	9.6
UGC 5750......	1.9	1.7	116.9	80.4	1.105	0.354	1.9	1.7	116.9	80.4	1.105	0.354	1.4
UGC 6614......	1.7	1.8	303.0	206.5	4.005	0.001	*0.4*	...	*145.6*	...	7.828	0.737	7.7
	SMT Data, Our Analysis												
F563-V2	6.5	3.8	136.0	73.3	1.047	0.397	*1.0*	...	350.0	...	0.449	0.878	4.1
F568-1	6.7	2.5	163.8	56.1	0.803	0.626	*0.6*	...	669.2	...	0.636	0.898	9.0
F568-3	*1.0*	...	*519.4*	...	3.595	0.000	*1.0*	...	467.8	...	3.624	0.000	1.8
F568-V1	14.6	1.4	88.8	5.3	0.228	0.998	3.3	1.5	125.8	45.7	0.222	0.998	14.0
F574-1	8.2	1.4	87.1	9.5	1.391	0.162	1.5	1.6	69.7	43.9	0.204	0.998	8.1

NOTE.—Italics indicate estimates, not actual fits. V_{200} is in kilometers per second.

TABLE 5
FITTING PARAMETERS: NFW HALO, SAMPLE II

| | MINIMUM DISK | | | | | |
GALAXY	c	Δc	V_{200}	ΔV	$\chi^2_{\rm red}$	p
F730-V1	11.8	1.9	131.4	16.2	0.995	0.426
UGC 4115	*5.0*	...	*133.4*	...	0.777	0.591
UGC 11454	10.4	2.0	152.6	23.3	3.334	0.000
UGC 11557	*1.0*	...	*425.1*	...	1.367	0.093
UGC 11583	*5.0*	...	*93.3*	...	0.676	0.641
UGC 11616	12.7	1.8	124.4	14.3	1.254	0.244
UGC 11648	8.0	0.7	146.2	10.9	0.964	0.498
UGC 11748	52.5	4.5	125.2	3.8	3.325	0.000
UGC 11819	6.4	1.9	252.9	77.6	1.348	0.177
ESO-LV 014-0040......	16.8	0.8	203.3	5.8	0.152	0.989
ESO-LV 084-0411......	*1.0*	...	*181.0*	...	1.608	0.077
ESO-LV 120-0211......	6.4	2.1	27.5	6.9	0.246	0.996
ESO-LV 187-0510......	3.8	1.5	93.6	38.6	0.059	1.000
ESO-LV 206-0140......	15.2	1.3	92.7	4.4	0.425	0.962
ESO-LV 302-0120......	6.6	1.5	98.5	18.4	0.333	0.965
ESO-LV 305-0090......	*1.0*	...	*323.6*	...	0.208	0.999
ESO-LV 425-0180......	3.1	0.9	301.6	77.8	0.014	1.000
ESO-LV 488-0490......	4.9	1.9	209.6	90.1	0.170	0.999

NOTE.—Italics indicate estimates, not actual fits. V_{200} is in kilometers per second.

This happened mostly with the NFW models. One of the reasons for this is that the inner parts of the rotation curves can be well described by $V(R) \sim R$, whereas the NFW model has the form $V \sim R^{1/2}$. To accommodate the model, the fit tries to stretch out the NFW curve (resulting in small c and high V_{200}) in order to make it *look* linear.

The second and fourth columns of panels in Figure 3 show the 1 σ (*thick contour*) and 2, 3, 4, and 5 σ (*thin contours*) probability contours of the halo parameters in logarithmic space. The reason for choosing a logarithmic representation is that the χ^2 distributions for the NFW halo parameters often show extended tails toward very small c, large V_{200}, or both. For comparison, Figure 4 shows a representative example of the σ-contours for the minimum disk model of F583-4 plotted in linear (c, V_{200})-space.

It is important to realize that the σ-contours are plotted *with respect to the minimum* χ^2. That is, existence of a narrow distribution only means that the minimum χ^2 is well defined. It does *not* imply that the fit is good in an absolute sense. For that, one needs to refer to the value of the reduced χ^2 itself or the probability p that the data and model are compatible. There are many cases in which the NFW model is not a good fit, making it difficult to plot absolute likelihood contours.

Finally, in the NFW contour plots in the second column, we show the range of c and V_{200} values for the currently popular ΛCDM cosmology as derived from numerical models (Navarro, Frenk, & White 1997; see § 5.3). The hatched and crosshatched areas shows the expected 2 σ and 1 σ logarithmic scatter in c (where $\sigma_c = 0.18$) as found in numerical models by Bullock et al. (2001). Independent simulations by Jing (2000) find a much smaller logarithmic scatter of $\sigma_c = 0.08$. The latter do of course put much stronger constraints on the NFW results. For the sake of clarity, however, and to give the NFW model as much chance as possible, we adopt the larger estimate of the scatter in c of Bullock et al. (2001).

For the pseudoisothermal halo, we show contours of constant central density ρ_0. The contours represent, from top to bottom, $\rho_0 = 0.1$ (*dotted line*), 1 (*dashed line*), 10, 100, and 1000 (*dotted lines*) $\times 10^{-3}$ $M_\odot$ pc^{-3}.

4.1. *Weighted versus Uniform*

To investigate how stable the derived halo parameters are with respect to the precise definition of the error bars, we have rederived the models assigning uniform and equal weights to all data points. Though we do not list the latter values here, we show in Figure 5 a comparison between the two sets of parameters. It is clear that these agree well, showing that the results presented here are robust against the precise definition of the error bars.

4.2. *Mass Models: Smooth and Raw*

Has the procedure used to derive the smooth rotation curves affected some of the model results? We established in § 2.3 that this procedure introduced no systematic differences between the smooth curves and the raw data. Here we test this again by checking whether the smooth curves give the same fit results as the raw data.

As the NFW model is more sensitive to changes in the inner slope than the pseudoisothermal model, we will use the former in our checks. We first fit NFW minimum disk models to the smooth and the raw curve of F583-1, as a representation of the data from Paper I. Both fits are presented in Figure 6, where we have imposed a minimum error of 4 km s^{-1} on the raw data to make the error bars consistent with the smooth curve. It is clear that the two fits are identical within the error bars. Similar results are obtained using other curves from Paper I.

As a second test, we evaluate the SMT data. We have fitted several minimum disk NFW models to each of the SMT galaxies. We have fitted the SMT raw data, the smooth curve presented in SMT, and our smooth curve derived from the raw SMT data. These fits were done inde-

TABLE 6

FITTING PARAMETERS: PSEUDOISOTHERMAL HALO, SAMPLE I

GALAXY	MINIMUM DISK						MINIMUM DISK PLUS GAS					
	R_C	ΔR	ρ_0	$\Delta\rho$	$\chi^2_{\rm red}$	p	R_C	ΔR	ρ_0	$\Delta\rho$	$\chi^2_{\rm red}$	p
F563-1	1.72	0.23	91.9	21.6	0.085	1.000	1.55	0.22	102.0	25.2	0.078	1.000
F568-3	2.92	0.36	36.6	5.4	0.522	0.860	2.71	0.39	38.3	6.8	0.676	0.731
F571-8	2.12	0.19	106.9	14.0	1.525	0.114	2.12	0.19	106.3	14.0	1.512	0.118
F579-V1	0.67	0.02	574.8	37.3	0.026	1.000	0.63	0.03	630.8	50.2	0.037	1.000
F583-1	2.44	0.06	33.0	1.1	0.037	1.000	2.08	0.11	37.7	2.5	0.117	1.000
F583-4	1.10	0.13	85.5	15.8	0.329	0.941	1.06	0.11	88.2	15.1	0.267	0.967
UGC 5750......	4.25	0.39	10.6	1.0	0.154	0.998	3.96	0.49	10.4	1.3	0.214	0.993
UGC 6614......	1.86	0.49	218.4	102.5	1.942	0.021	1.73	0.44	244.7	111.6	1.777	0.040
SMT Data, Our Analysis												
F563-V2	1.69	0.17	131.2	19.4	0.283	0.972	1.58	0.20	135.3	24.7	0.393	0.925
F568-1	2.22	0.10	97.2	6.2	0.066	1.000	2.03	0.12	104.6	8.9	0.106	1.000
F568-3	3.93	0.75	30.2	5.6	1.256	0.245	3.75	0.78	30.8	6.3	1.383	0.173
F568-V1	1.45	0.11	153.0	18.2	0.110	1.000	1.33	0.14	170.0	27.8	0.172	1.000
F574-1	1.83	0.06	71.5	3.7	0.100	1.000	1.70	0.09	76.9	6.3	0.232	0.997

GALAXY	CONSTANT $\Upsilon_*(R) = 1.4$						MAXIMUM DISK						
	R_C	ΔR	ρ_0	$\Delta\rho$	$\chi^2_{\rm red}$	p	R_C	ΔR	ρ_0	$\Delta\rho$	$\chi^2_{\rm red}$	p	Υ_*^R
F563-1	1.72	0.26	79.0	21.3	0.083	1.000	4.09	1.01	13.2	4.9	0.124	0.998	6.9
F568-3	3.07	0.63	25.7	6.3	0.793	0.623	3.36	0.88	19.7	5.9	0.89	0.536	2.2
F571-8	4.19	0.28	34.4	2.7	0.405	0.954	9.97	3.43	9.8	2.3	2.639	0.002	4.2
F579-V1	0.55	0.04	694.4	84.0	0.06	1.000	0.17	0.16	1970	3234	1.032	0.415	7.9
F583-1	2.26	0.11	31.5	2.0	0.103	1.000	3.41	0.24	14.3	1.2	0.121	1.000	6.5
F583-4	1.02	0.12	80.6	15.2	0.249	0.972	0.23	0.15	103.4	114.1	0.188	0.988	9.6
UGC 5750......	4.67	0.74	7.1	1.1	0.262	0.984	4.67	0.74	7.1	1.1	0.262	0.984	1.4
UGC 6614......	12.18	2.87	6.3	1.9	1.938	0.022	112.0	506.7	0.4	0.4	4.762	0.000	7.4
SMT Data, Our Analysis													
F563-V2	1.70	0.24	96.6	19.8	0.298	0.967	2.32	0.63	30.8	11.5	0.191	0.992	4.1
F568-1	2.11	0.15	90.7	9.0	0.120	1.000	3.08	0.73	27.6	8.5	0.270	0.988	9.0
F568-3	4.35	1.31	21.5	6.0	1.709	0.065	4.54	1.52	19.4	5.9	1.815	0.046	1.8
F568-V1	1.41	0.15	146.1	23.0	0.153	1.000	3.80	0.58	14.8	2.6	0.120	1.000	14.0
F574-1	1.74	0.09	63.1	5.4	0.182	0.999	3.30	0.83	4.6	1.6	0.108	1.000	8.1

NOTE.—R_C is in kiloparsecs; ρ_0 is expressed in units of $10^{-3} M_\odot \, {\rm pc}^{-3}$.

pendently by two of us using independent fit codes on the smoothed (W. J. G. d. B.) and unsmoothed (S. S. M.) data. Table 8 lists the derived parameter values. For comparison, we also list the results for our own independent observation of F568-3 from Paper I. In Figure 7 we compare the c-values derived for each galaxy.

One can see that the galaxies for which our smooth curves and those presented in SMT agree also have similar model parameters, which agree with those derived from the raw data (F574-1 and F568-V1). In the other three cases (F563-V2, F568-1, F568-3), the c-values derived from our version of the smooth curves agree with those derived from the raw data, whereas the SMT c-values are higher. It is important to keep in mind that even though the formal fit values show a large discrepancy, the rotation curves themselves only show very subtle differences (Fig. 2). This illustrates the importance of having high-accuracy rotation curves of a large sample. In the following we only consider our smooth versions of the SMT data.

In summary, we believe that the results from our smooth curves are not systematically different from the raw data. As

stated before, we prefer to use the smooth curves, as these are more evenly sampled and prevent the occurrence of imaginary halo masses that can arise when the occasional (raw) data point happens to scatter below the rotation velocity of the disk alone.

4.3. Remarks on Individual Galaxies

F563-1: For this galaxy, independent observations are available from de Blok & Bosma (2001; see Paper I for a comparison). Note that the observed curve differs significantly from the "beam-smearing corrected" model presented in van den Bosch et al. (2000). The model presented there shows an almost flat rotation curve over most of the radial range, which clearly disagrees with the new data. Beam-smearing corrections are not infallible.

F563-V2: This is our version of one of the SMT curves. This curve does significantly worse at fitting NFW than a pseudoisothermal halo. The systematics seen here is typical for many of the NFW fits: the inner parts are overestimated; the model then underestimates the middle parts and shoots up again in the outer parts. For this galaxy no

TABLE 7
FITTING PARAMETERS: PSEUDOISOTHERMAL HALO, SAMPLE II

| | | | | MINIMUM DISK | | |
GALAXY	R_C	ΔR	ρ_0	$\Delta\rho$	χ^2_{red}	p
F730-V1	1.46	0.06	215.8	14.2	0.097	0.997
UGC 4115	0.94	0.03	148.2	2.4	0.004	1.000
UGC 11454	1.95	0.10	146.9	11.8	0.423	0.927
UGC 11557	5.48	0.55	15.2	0.9	0.052	1.000
UGC 11583	0.63	0.08	117.8	16.5	0.103	0.999
UGC 11616	1.45	0.05	208.9	11.6	0.140	1.000
UGC 11648	1.95	0.25	104.9	20.7	3.792	0.000
UGC 11748	0.36	0.15	8540	6661	5.402	0.000
UGC 11819	2.93	0.14	88.2	5.2	0.303	0.991
ESO-LV 014-0040......	2.55	0.18	249.5	27.0	0.176	0.982
ESO-LV 084-0411......	6.41	0.56	5.2	0.3	0.067	0.999
ESO-LV 120-0211......	0.57	0.08	45.5	9.2	0.082	1.000
ESO-LV 187-0510......	0.97	0.05	53.5	3.2	0.028	1.000
ESO-LV 206-0140......	1.17	0.05	231.1	16.9	0.106	1.000
ESO-LV 302-0120......	1.90	0.09	53.6	3.4	0.035	1.000
ESO-LV 305-0090......	2.09	0.14	27.3	1.8	0.048	1.000
ESO-LV 425-0180......	4.41	0.75	30.0	6.6	0.088	0.997
ESO-LV 488-0490......	1.63	0.04	101.1	3.1	0.016	1.000

NOTE.—R_C is in kiloparsecs; ρ_0 is expressed in units of $10^{-3} M_\odot \text{ pc}^{-3}$.

R-band photometry is available, and we have used B-band photometry from McGaugh & Bothun (1994). Assuming $B-R = 0.9$, which is the typical color for an LSB galaxy, this yields a value for the constant-Υ_* case of $\Upsilon_*(B) = 1.1$. The maximum disk NFW model fits significantly better than the other NFW models. It is however not compatible with cosmological predictions from the numerical models.

F568-1: This is another of the curves presented by SMT. The systematics of overestimating the inner part, underestimating the middle, and overestimating the outer velocities

again is also present here. Again maximum disk is the best of the NFW models, which is another way of saying that the shapes of the (inner) rotation curves are more like that expected for the stars (albeit with the wrong Υ_*).

F568-3: This is a well-determined curve, for which there are several consistent independent measurements (see Paper I).

F571-8: This is the only edge-on galaxy in sample I, so we are concerned about optical depth and projection effects in the optical data. (The H I data are not used for this galaxy.)

TABLE 8
COMPARISON OF FITTING PARAMETERS

| | | | NFW HALO, MINIMUM DISK | | | | |
GALAXY	OBS.	CURVE	c	Δc	V_{200}	ΔV_{200}	χ^2_{red}
F563-V2....	SMT	SMT	16.2	3.4	84.5	10.4	2.516
		dBMR	7.5	3.7	153.1	70.5	1.391
		Data	5.9	2.2	192.3	76.4	3.42
F568-1......	SMT	SMT	13.4	1.1	112.1	6.3	0.265
		dBMR	6.4	2.5	194.6	71.9	0.804
		Data	8.3	1.1	154.5	18.5	3.49
F568-3......	SMT	SMT	5.1	2.9	160.3	88.0	2.147
		dBMR	*1.17*	...	*591.0*	...	3.551
		Data	1.71	0.5	400.4	94.8	13.9
	Paper I	dBMR	3.2	3.7	214.6	233.9	2.239
		Data[a]	4.6	0.5	168.4	17.7	8.01
F568-V1....	SMT	SMT	14.2	0.7	91.5	2.3	0.239
		dBMR	14.6	1.2	92.1	4.9	0.197
		Data	15.8	1.1	85.7	3.8	12.7
F574-1......	SMT	SMT	9.4	0.7	91.2	4.3	0.421
		dBMR	8.3	1.3	98.3	10.4	1.595
		Data	8.2	0.4	99.3	3.4	3.84

NOTE.—Italics indicate estimates, not actual fits. V_{200} is in kilometers per second. The column labeled "Obs." gives the source of the raw data. The column labeled "Curve" gives the source for the derived rotation curve: "SMT" indicates smooth rotation curve from Swaters et al. 2000; "dBMR" indicates smooth rotation curve from this paper; "Data" indicates a fit to the raw data.
[a] Uncertain, depends on initial estimates of fit.

F563-1, NFW halo
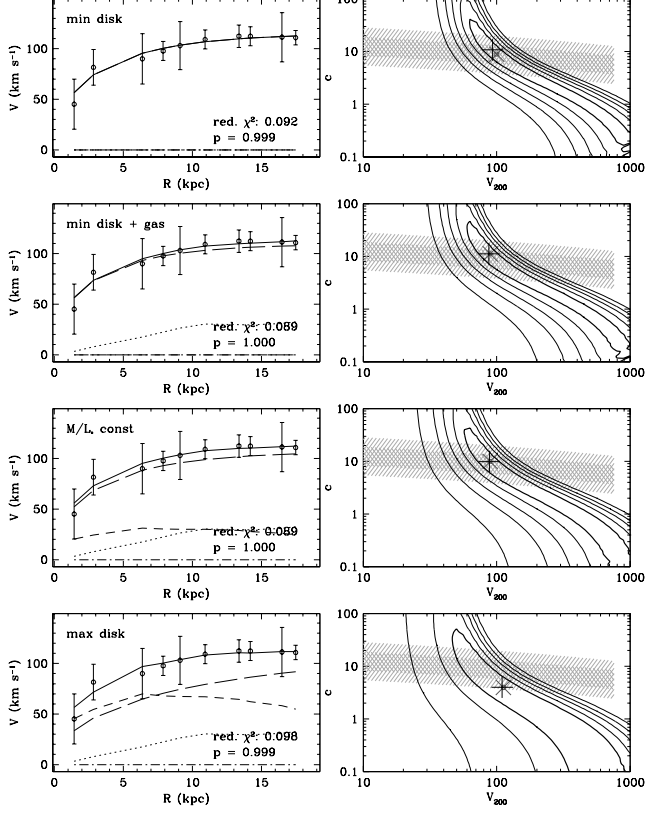
F563-1, ISO halo
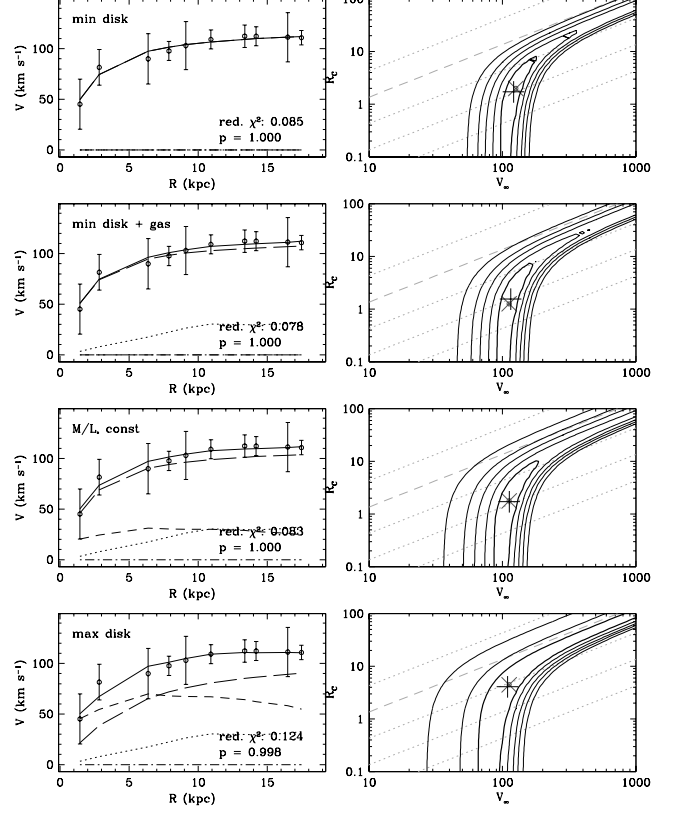
F563-V2, NFW halo
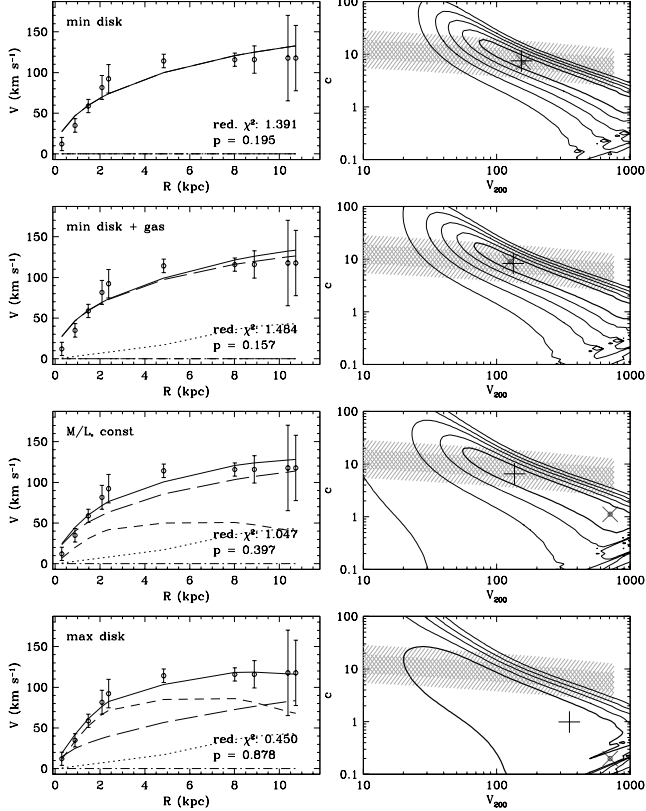
F563-V2, ISO halo
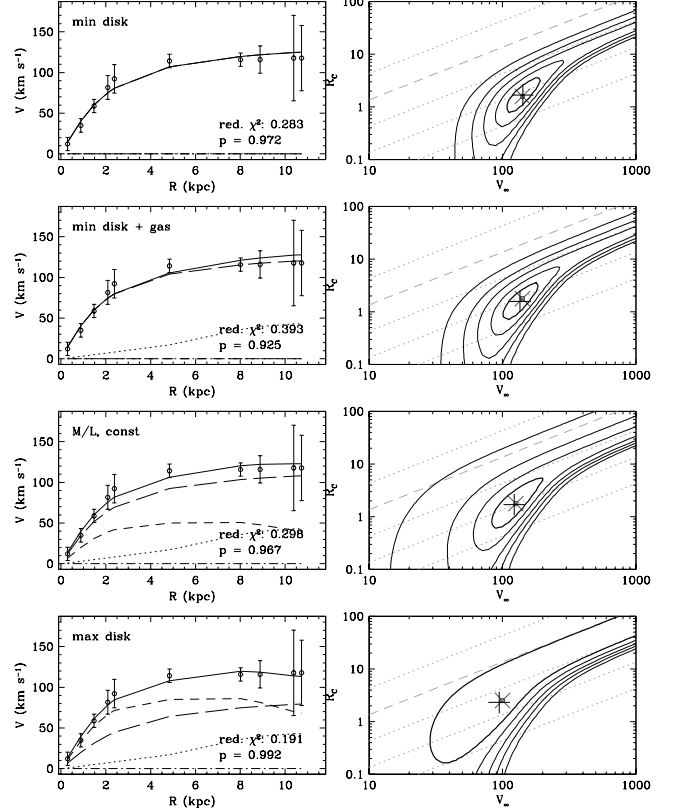
Fig. 3.—Mass models assuming NFW halo (*left*) and pseudoisothermal halo (*right*). For each halo model, the left column shows the best-fitting model, and the right column shows the probability distribution of the halo parameters. For a full description, see § 4.

F568-1, NFW halo
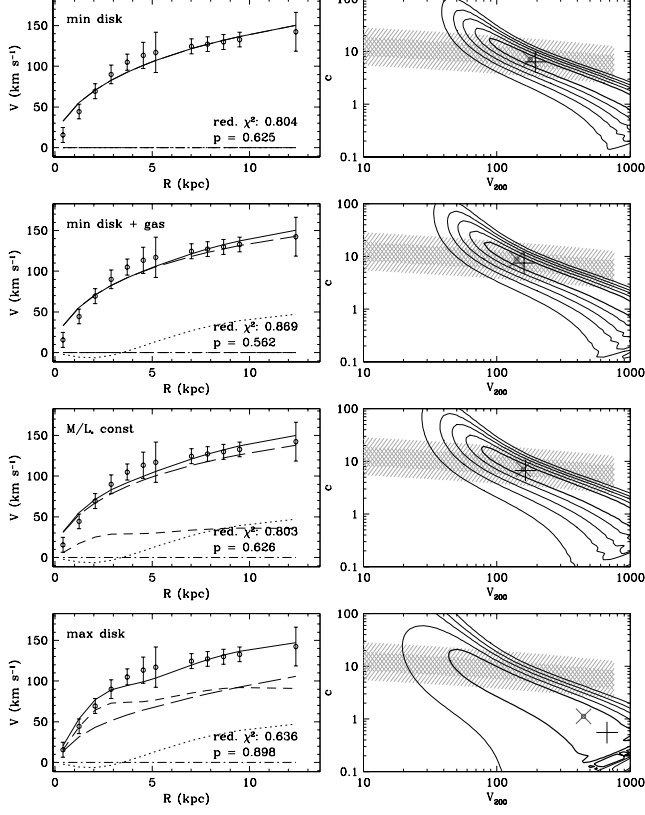
F568-1, ISO halo
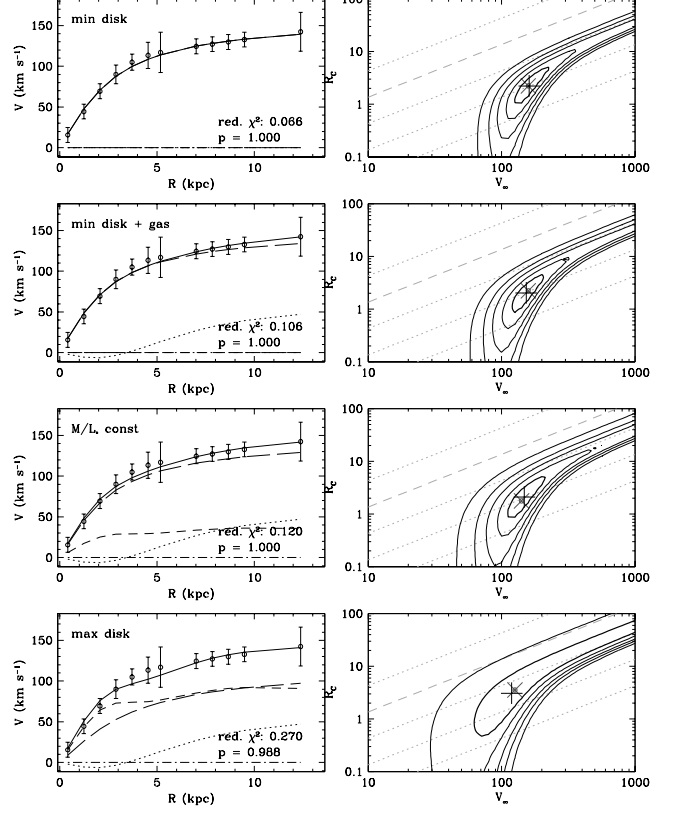
F568-3, NFW halo
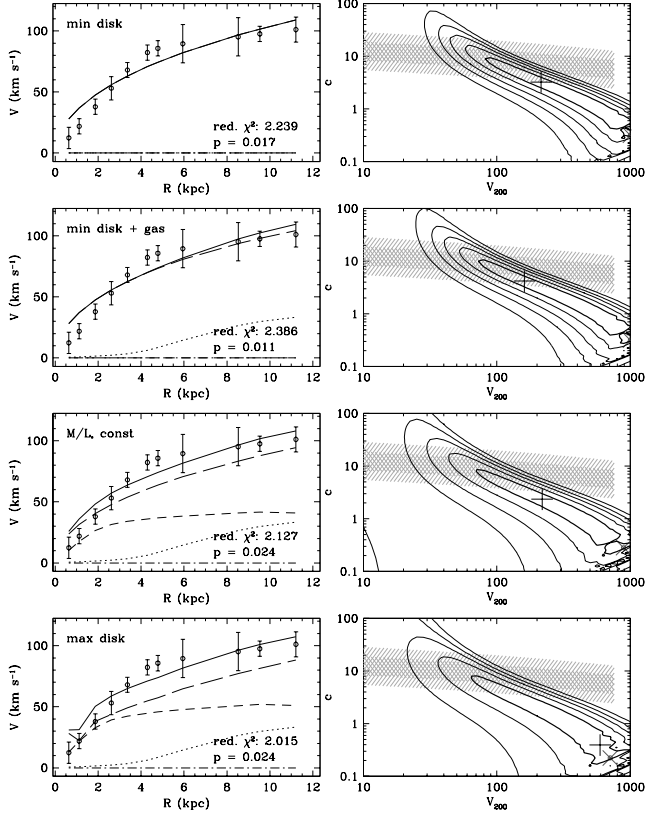
F568-3, ISO halo
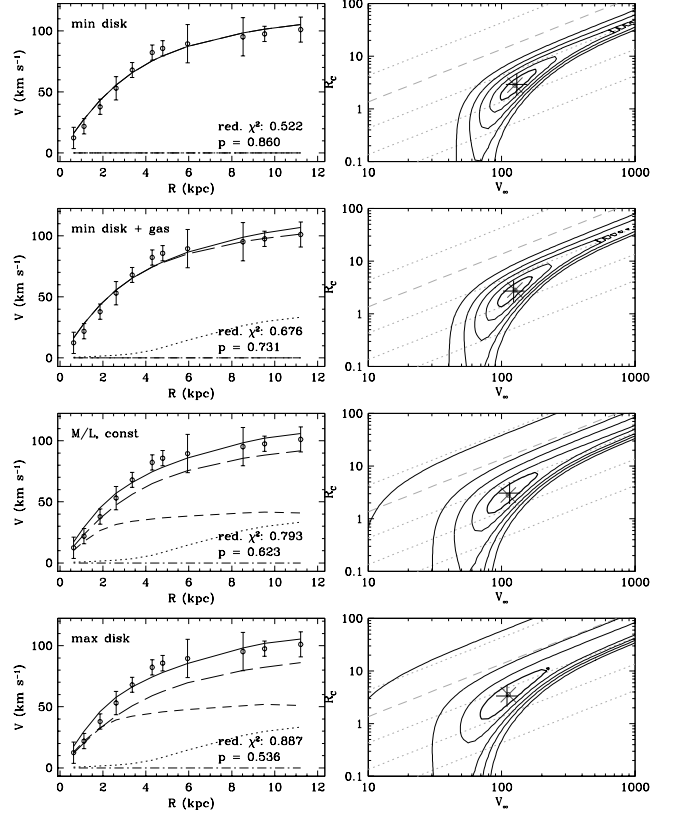
FIG. 3.—*Continued*

F568-3(STM), NFW halo
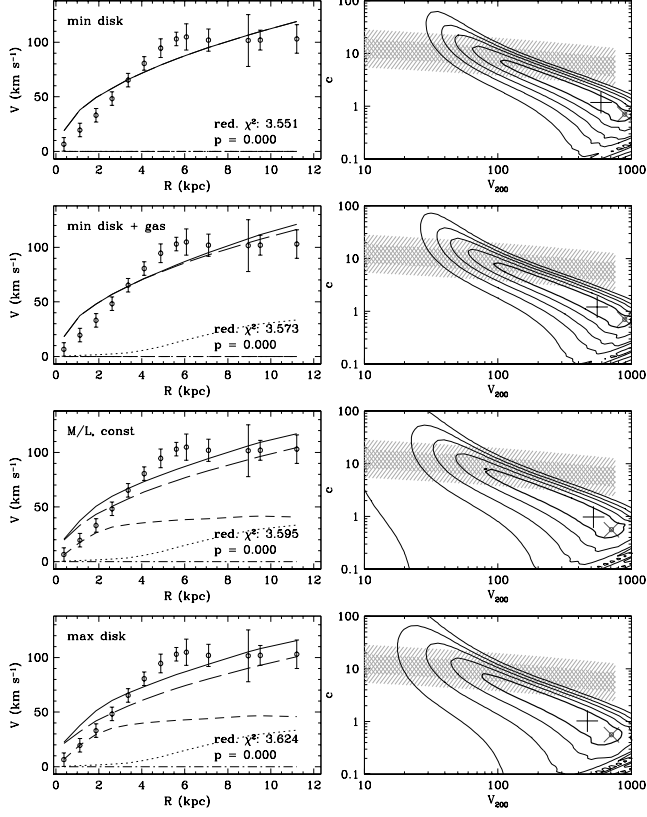
F568-3(STM), ISO halo
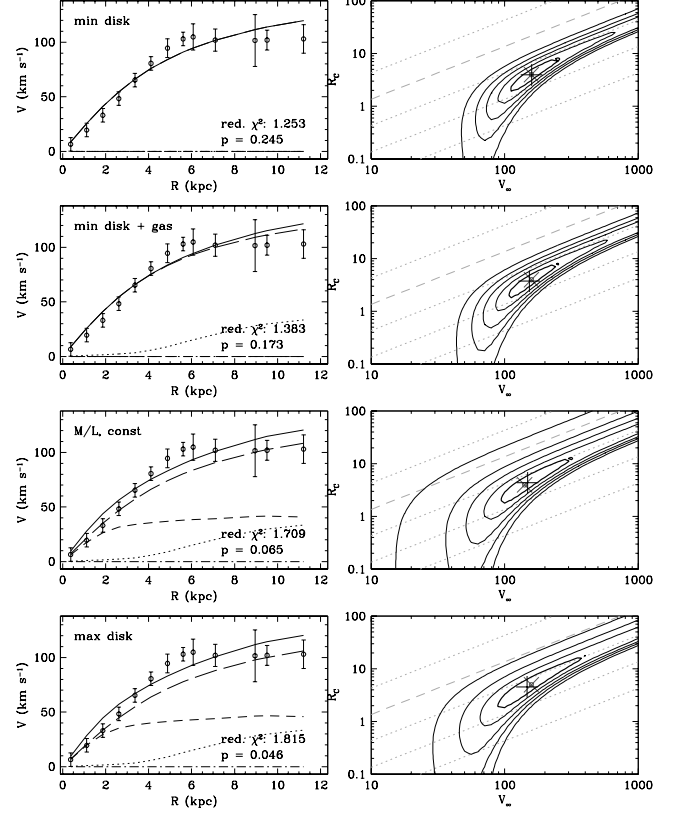
F568-V1, NFW halo
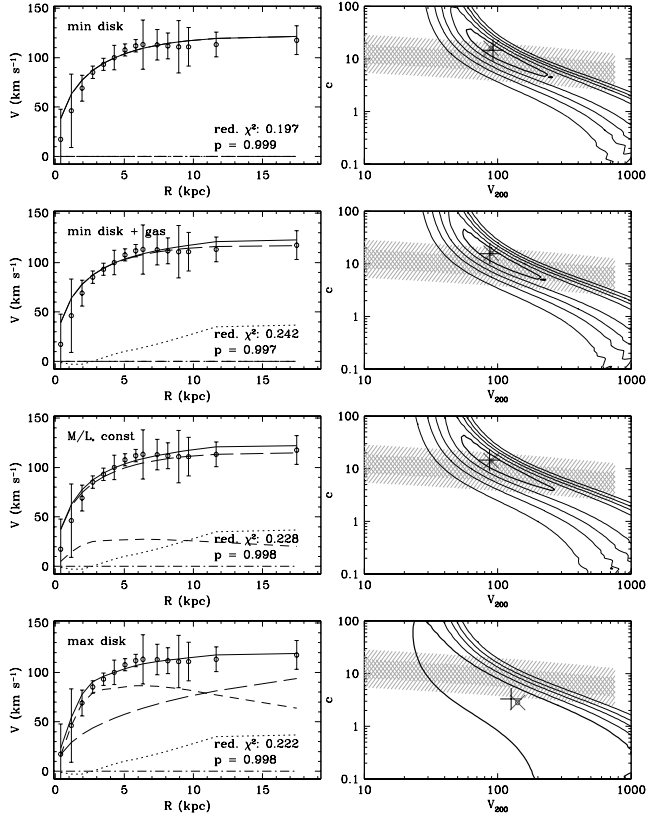
F568-V1, ISO halo

Fig. 3.—*Continued*

2409
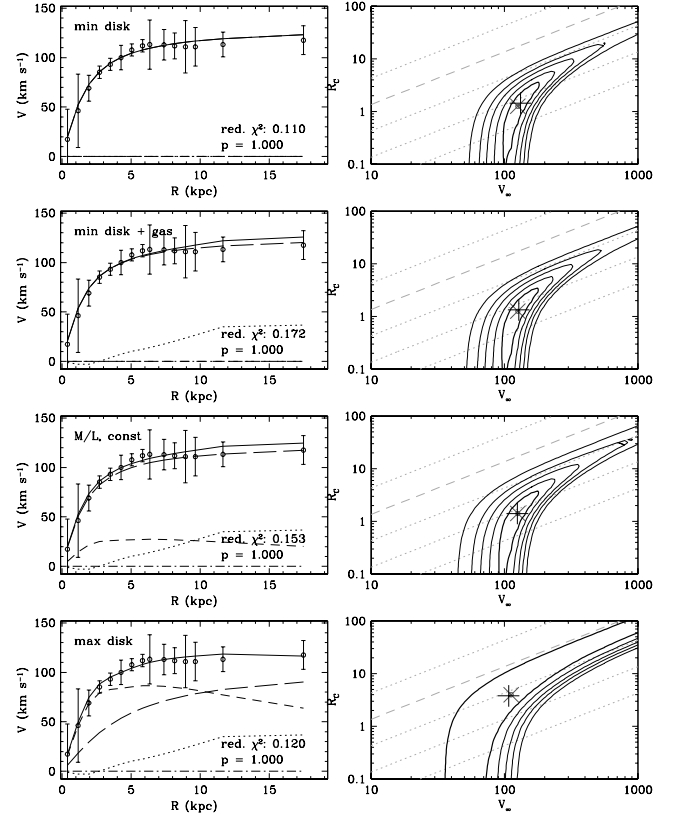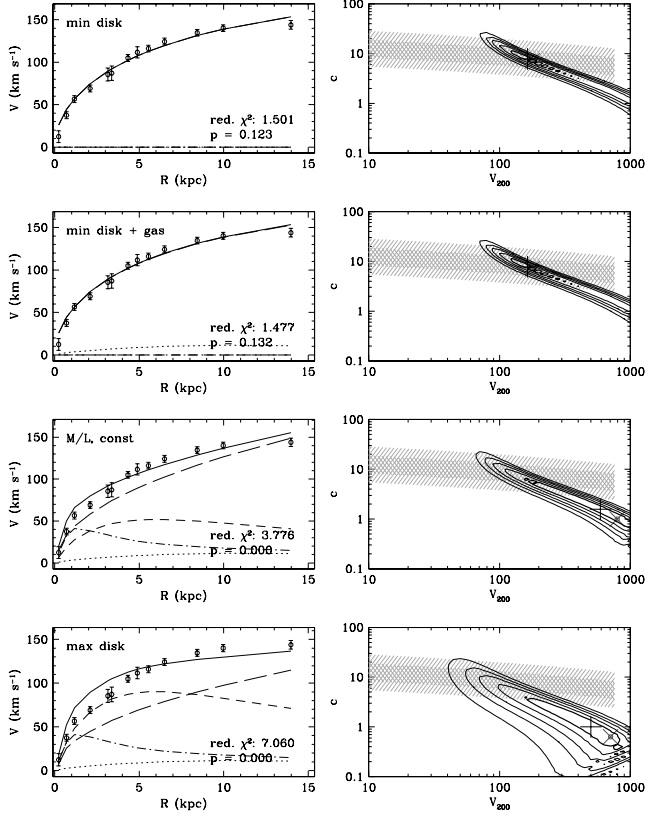
F571-8, NFW halo

F571-8, ISO halo
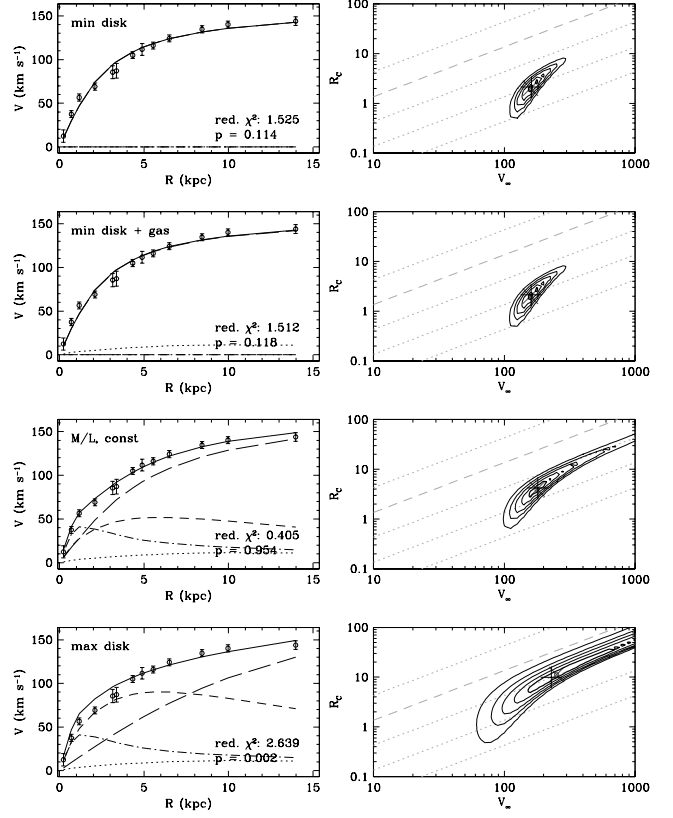
F574-1, NFW halo
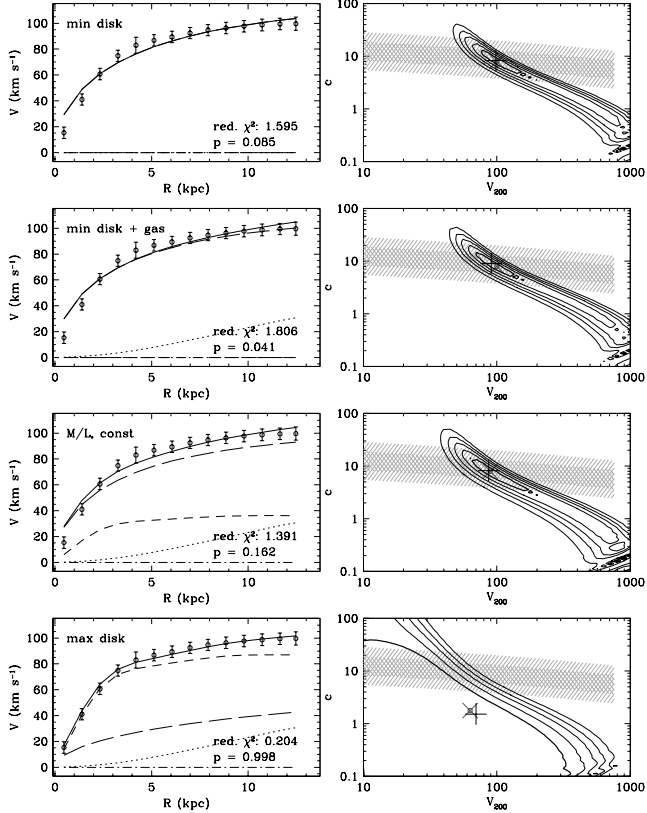
F574-1, ISO halo
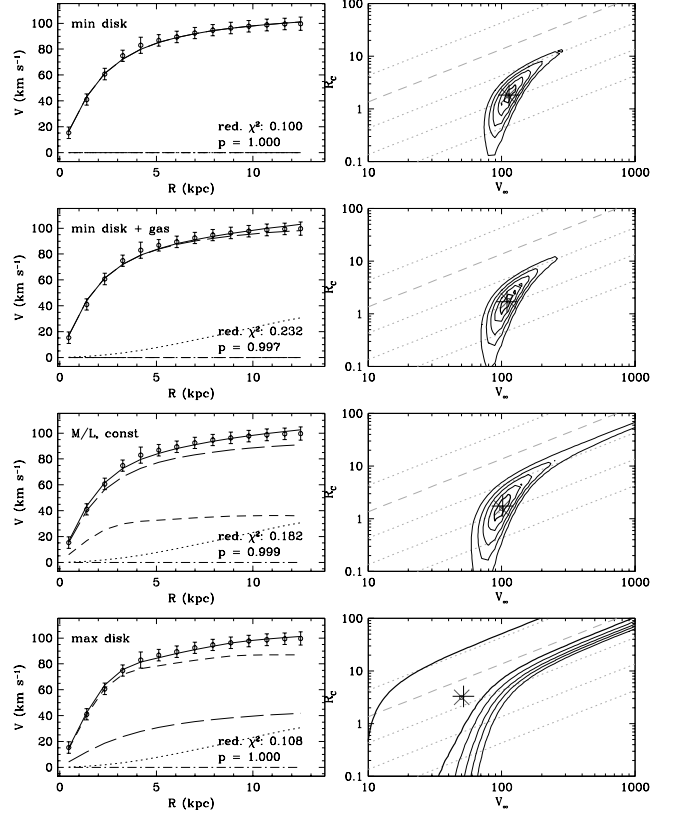
FIG. 3.—*Continued*

F579−V1, NFW halo

min disk

red. χ²: 0.211
p = 0.998

min disk + gas

red. χ²: 0.217
p = 0.998

M/L, const

red. χ²: 0.215
p = 0.998

max disk

red. χ²: 0.671
p = 0.781

F579−V1, ISO halo

min disk

red. χ²: 0.026
p = 1.000

min disk + gas

red. χ²: 0.037
p = 1.000

M/L, const

red. χ²: 0.065
p = 1.000

max disk

red. χ²: 1.032
p = 0.415

F583−1, NFW halo

min disk

red. χ²: 0.740
p = 0.746

min disk + gas

red. χ²: 0.827
p = 0.648

M/L, const

red. χ²: 0.767
p = 0.716

max disk

red. χ²: 0.680
p = 0.804

F583−1, ISO halo

min disk

red. χ²: 0.037
p = 1.000

min disk + gas

red. χ²: 0.117
p = 1.000

M/L, const

red. χ²: 0.103
p = 1.000

max disk

red. χ²: 0.121
p = 1.000

Fig. 3.—*Continued*

F583-4, NFW halo
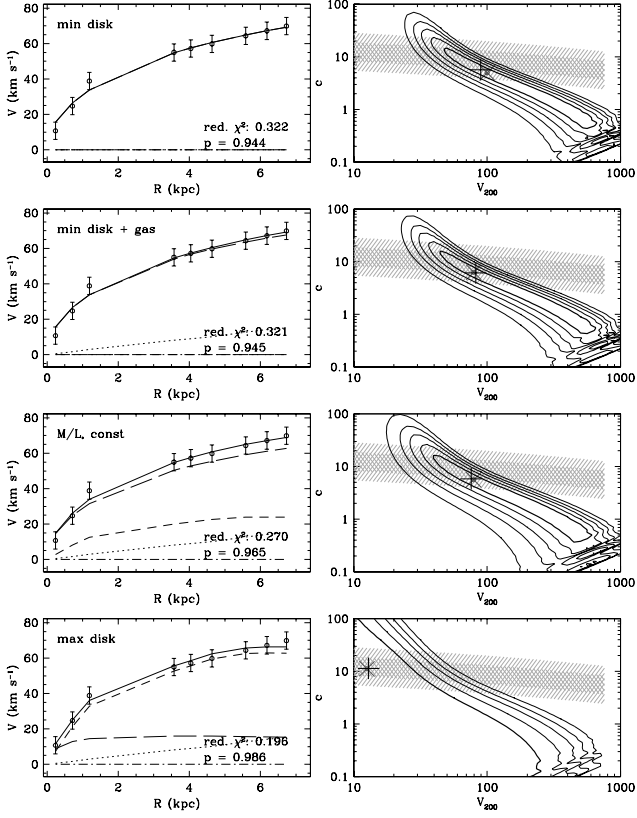
F583-4, ISO halo
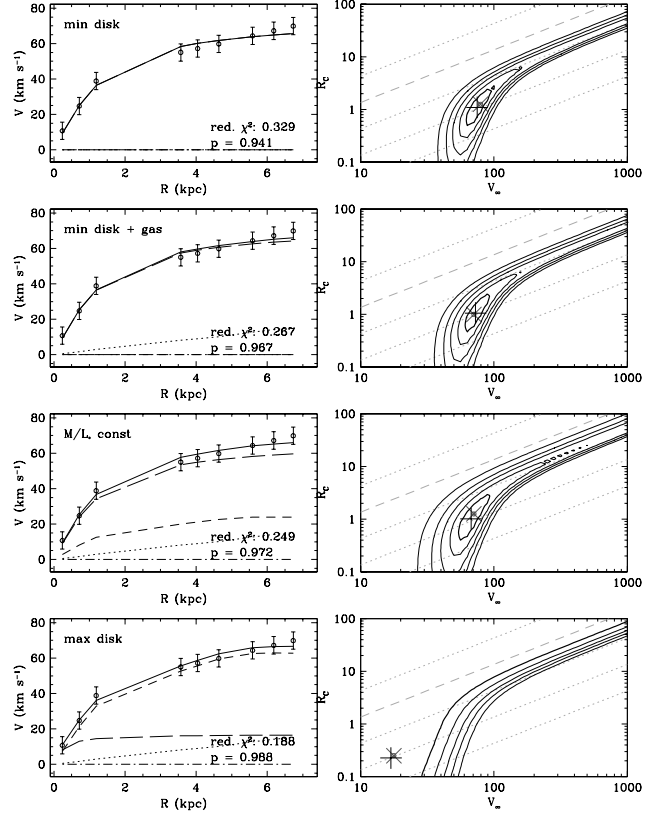
U5750, NFW halo
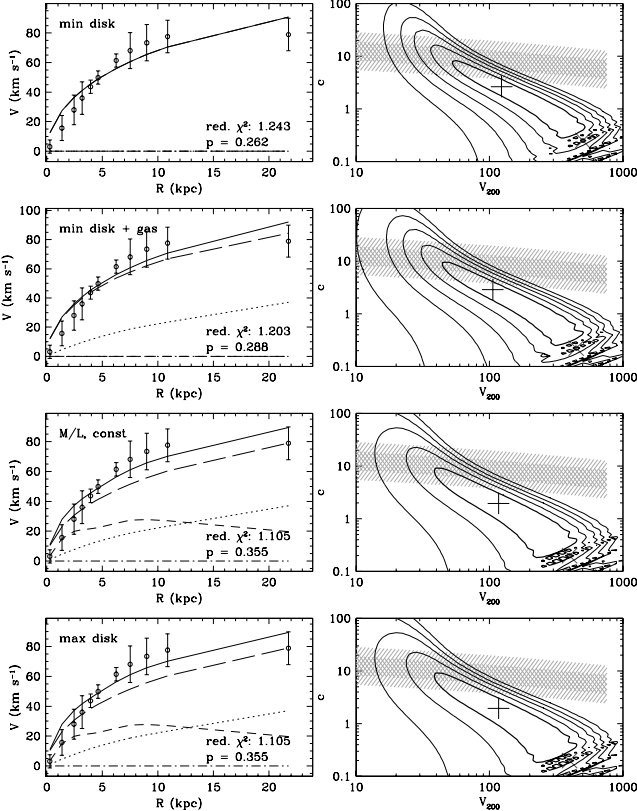
U5750, ISO halo
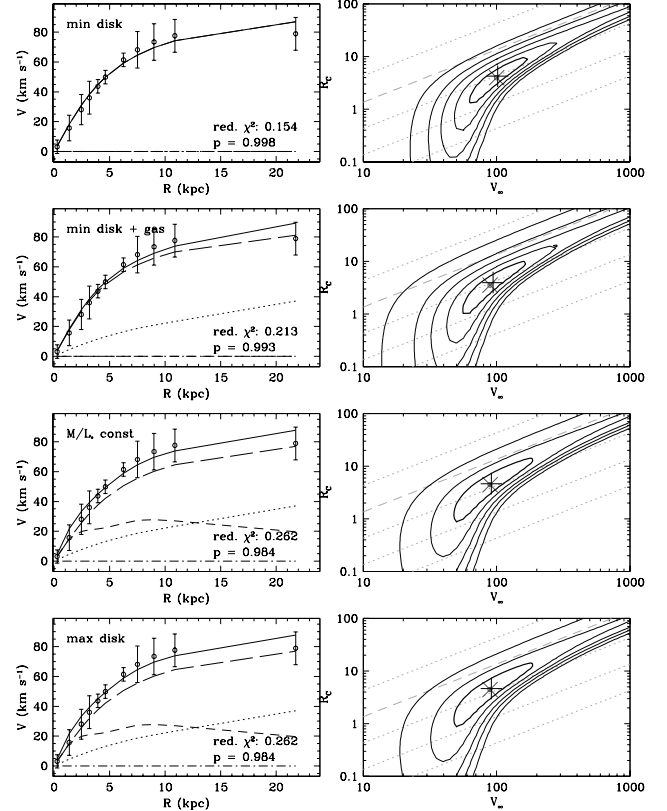
Fig. 3.—*Continued*

U6614, NFW halo
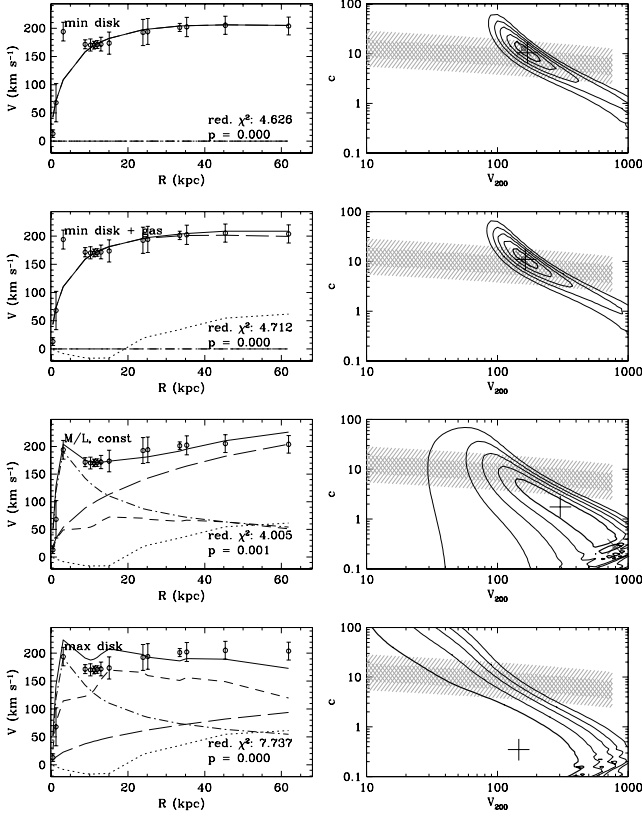
U6614, ISO halo
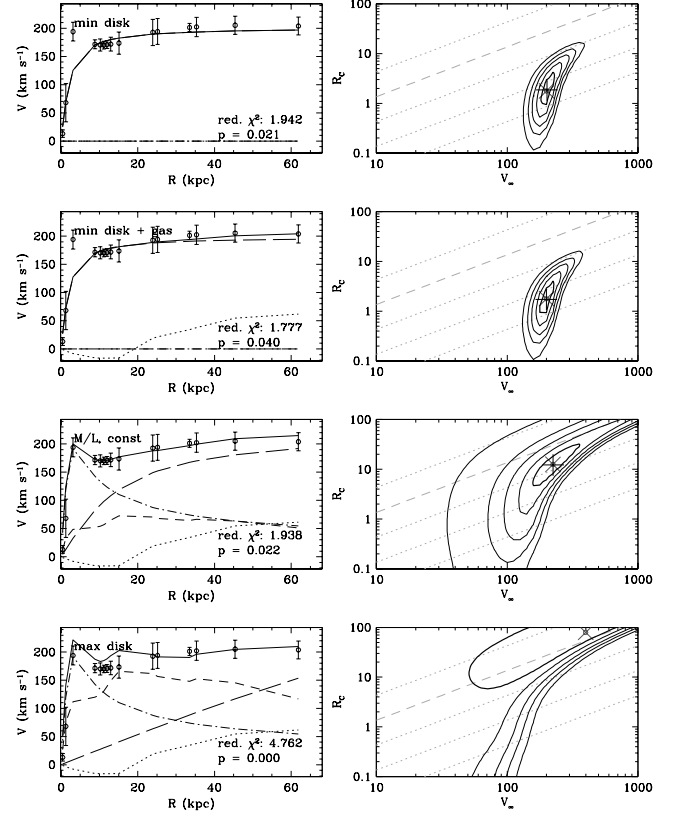
F730−V1, NFW halo
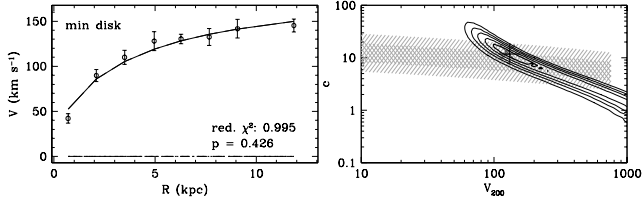
F730−V1, ISO halo
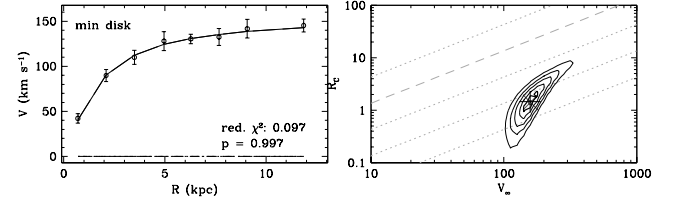
U4115, NFW halo
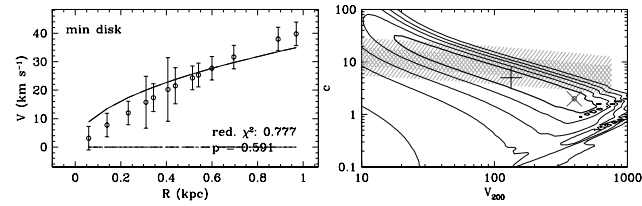
U4115, ISO halo
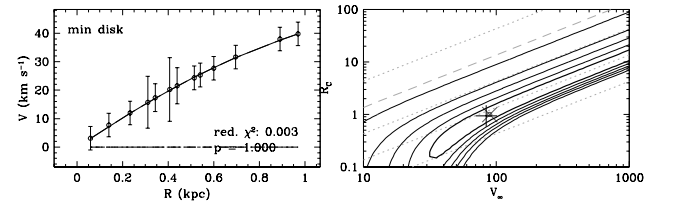
U11454, NFW halo
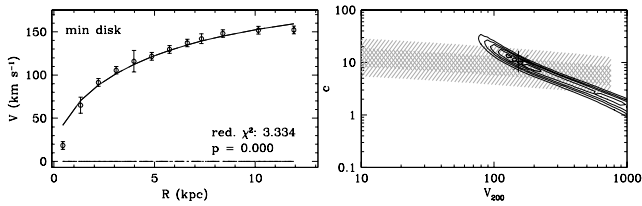
U11454, ISO halo

FIG. 3.—*Continued*

2413
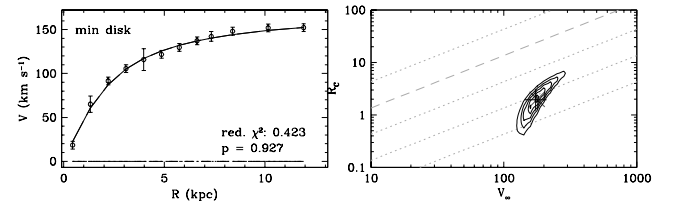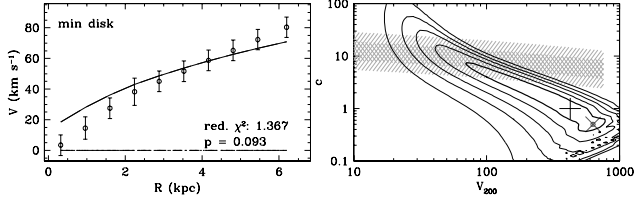
U11557, NFW halo

U11557, ISO halo
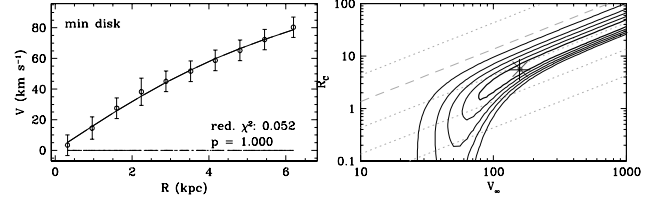
U11583, NFW halo
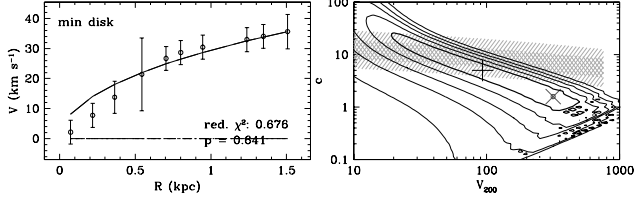
U11583, ISO halo
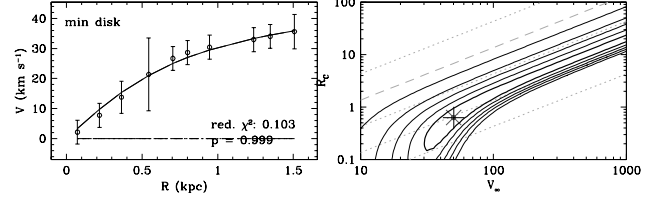
U11616, NFW halo
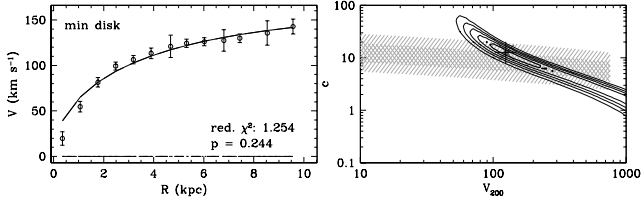
U11616, ISO halo
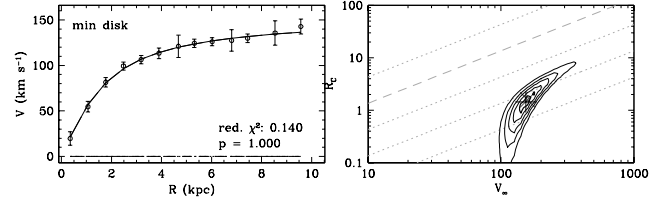
U11648, NFW halo
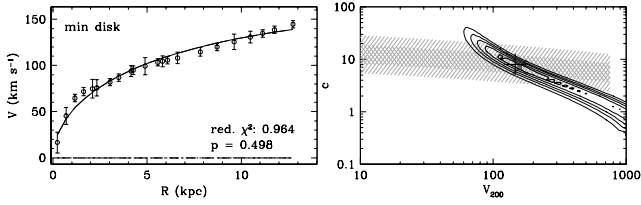
U11648, ISO halo
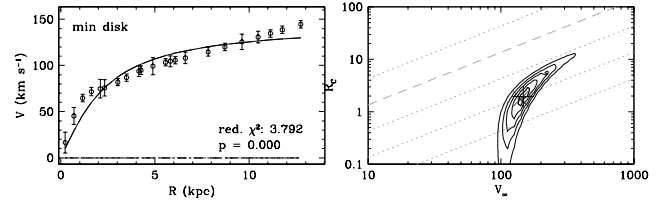
U11748, NFW halo
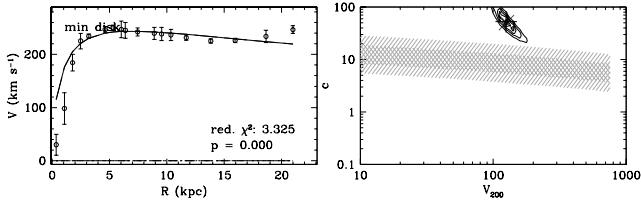
U11748, ISO halo
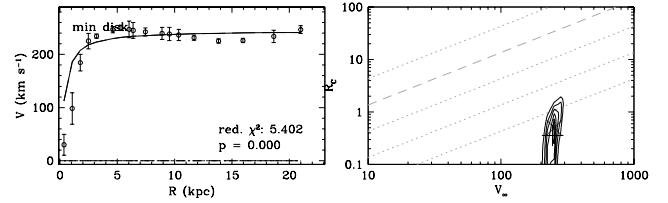
U11819, NFW halo
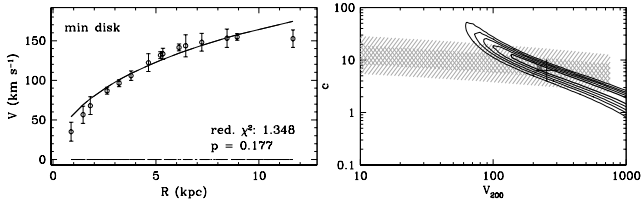
U11819, ISO halo

Fig. 3.—*Continued*

2414
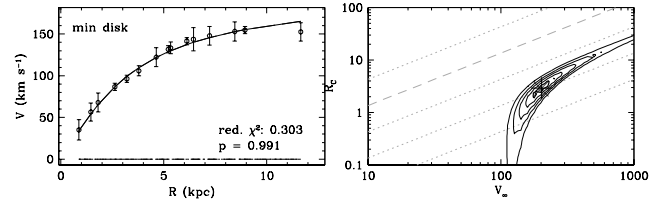
ESO0140040, NFW halo
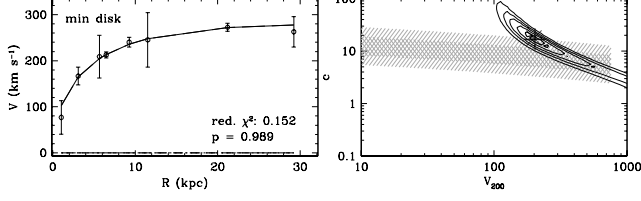
ESO0140040, ISO halo
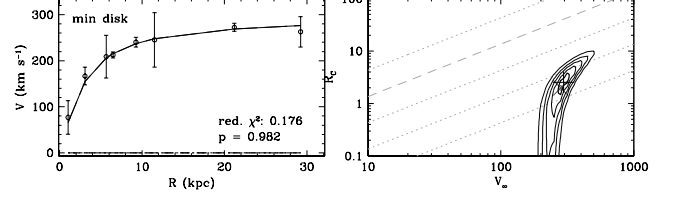
ESO0840411, NFW halo
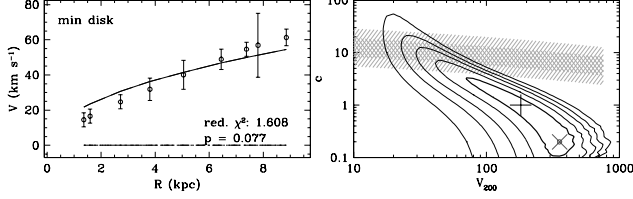
ESO0840411, ISO halo
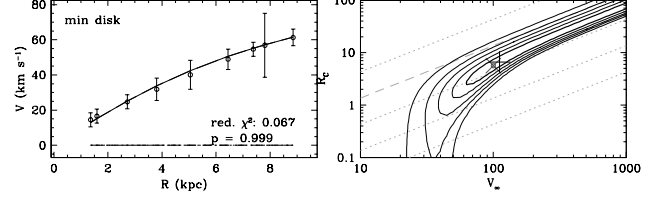
ESO1200211, NFW halo
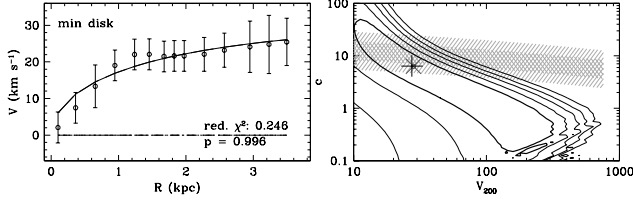
ESO1200211, ISO halo
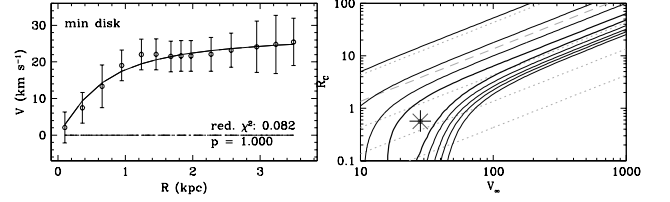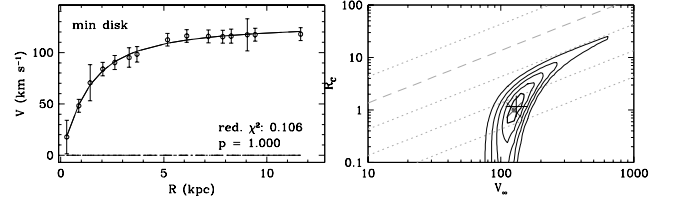
ESO1870510, NFW halo
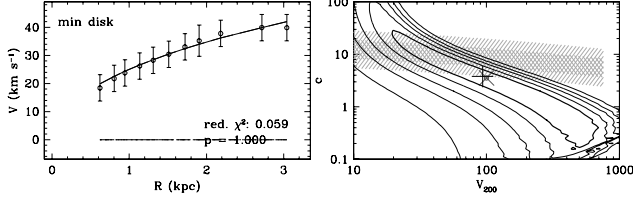
ESO1870510, ISO halo
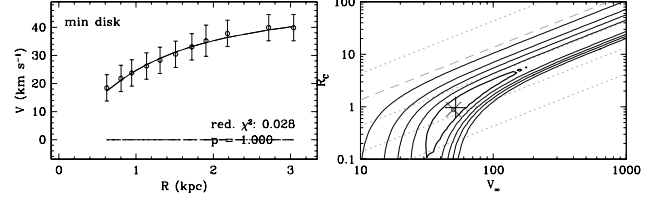
ESO2060140, NFW halo
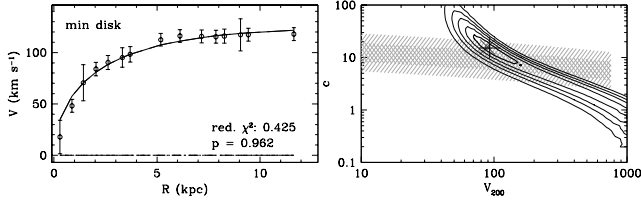
ESO2060140, ISO halo

ESO3020120, NFW halo
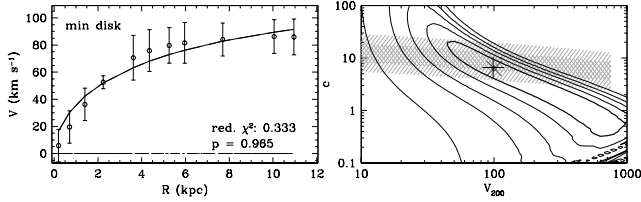
ESO3020120, ISO halo

FIG. 3.—*Continued*

2415

ESO3050090, NFW halo

ESO3050090, ISO halo

ESO4250180, NFW halo

ESO4250180, ISO halo

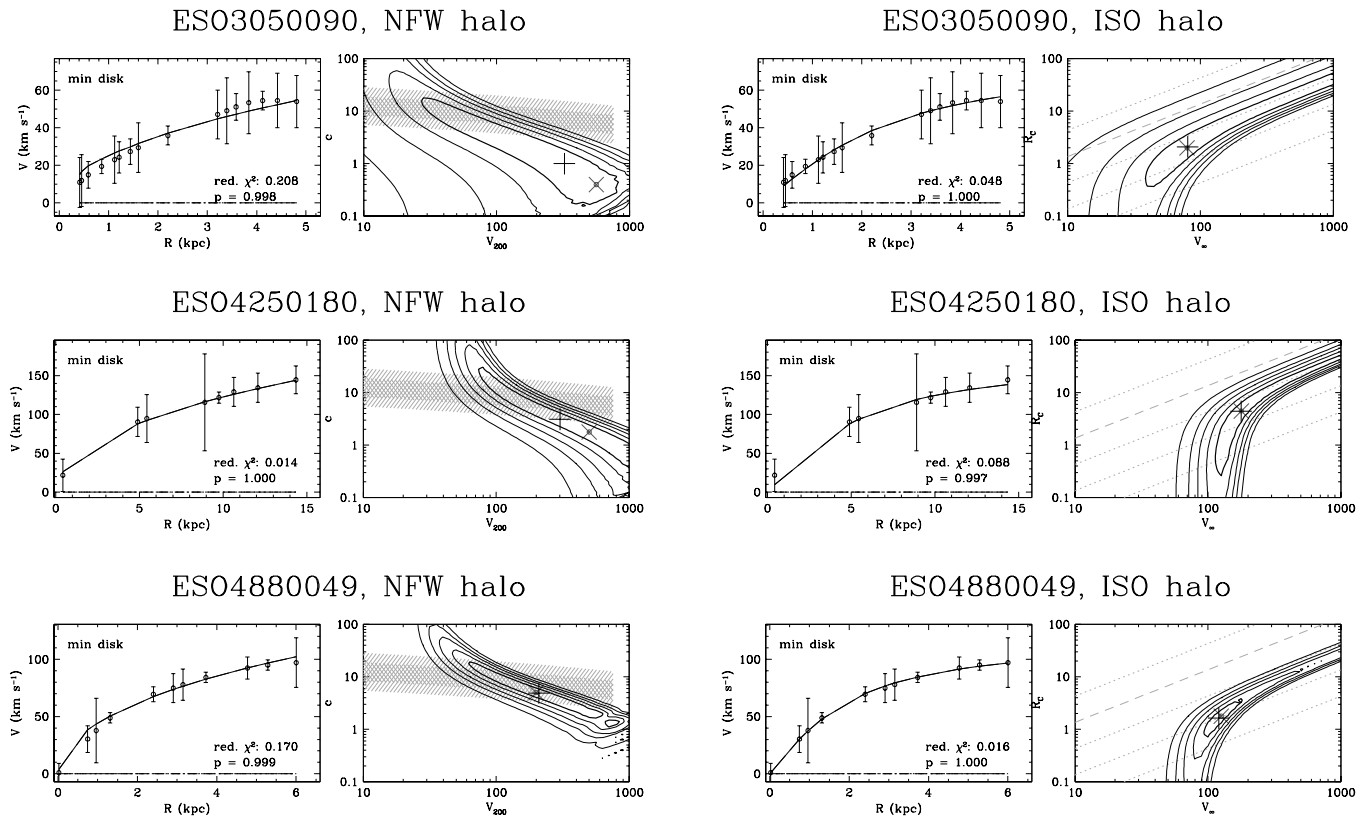## ESO4880049, NFW halo

ESO4880049, ISO halo
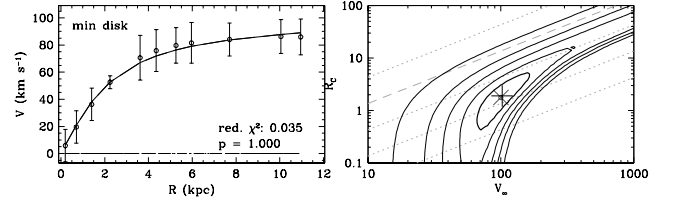
FIG. 3.—*Continued*

These effects could cause us to measure the rotation velocity at a ring where the optical depth becomes unity. Recently, Matthews & Wood (2001) have used radiative transfer models to investigate optical depth effects on rotation curves in edge-on LSB galaxies, and they conclude that these effect are likely to be small because of the low dust content in LSB galaxies. Bosma et al. (1992), in a comparison of the optical and H I curves of the edge-on galaxy

NGC 100, also found that late-type galaxies tend to be transparent, even when seen edge-on. Nevertheless, we cannot exclude the possibility that the shape of the optical curve is affected. If this is so, then *in this case* the mass model will change. For the constant-Υ_* and maximum disk cases we have added an exponential bulge with $\Upsilon_*(R)_{bulge} = 0.5$ (see BMH for a description of the bulge-disk decomposition).

F574-1: Another SMT curve. While the pseudoisothermal halo fits for this galaxy are good, the NFW fits show the by now familiar discrepancy: too steep in the inner part, underestimating the middle, and rising too quickly in the outer parts. Maximum disk NFW provides a good fit, albeit with low c and high Υ_*. F574-1 was the worst case of beam smearing from the H I sample, but the increase in the initial rate of rise of the rotation curve found optically does not really help NFW. The optical data imply a "cusp" slope ($\rho \propto r^\alpha$) of $\alpha = -0.49 \pm 0.26$ (de Blok et al. 2001), still well short of the NFW value $\alpha = -1$. This is the limit in the minimum disk case; if allowance is made for stellar mass, a value even closer to a constant-density core is required.

F583-1: A well-resolved and well-observed curve that shows the NFW over-/under-/overfit discrepancy. For all assumptions about stellar mass, $\chi^2_{iso} \ll \chi^2_{NFW}$. This galaxy strongly prefers a halo with a constant-density core over one with a cusp, a conclusion that has not changed from McGaugh & de Blok (1998). Only a substantial change in the shape of the rotation curve would alter this conclusion, which would require a large *systematic* error. Beam smearing can no longer be invoked as the cause of such a systematic error now that this object has been resolved to subkiloparsec scales.

UGC 5750: This curve was observed both by us and by de Blok & Bosma (2001), and the two data sets show good
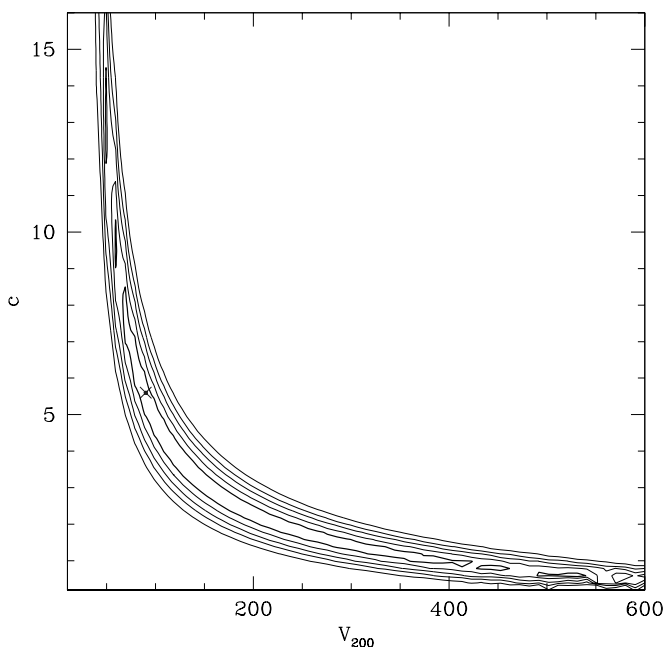

FIG. 4.—Error contours for the minimum disk NFW fit of F583-4 drawn in linear (c, V_{200})-space. Contour values are as in Fig. 3.
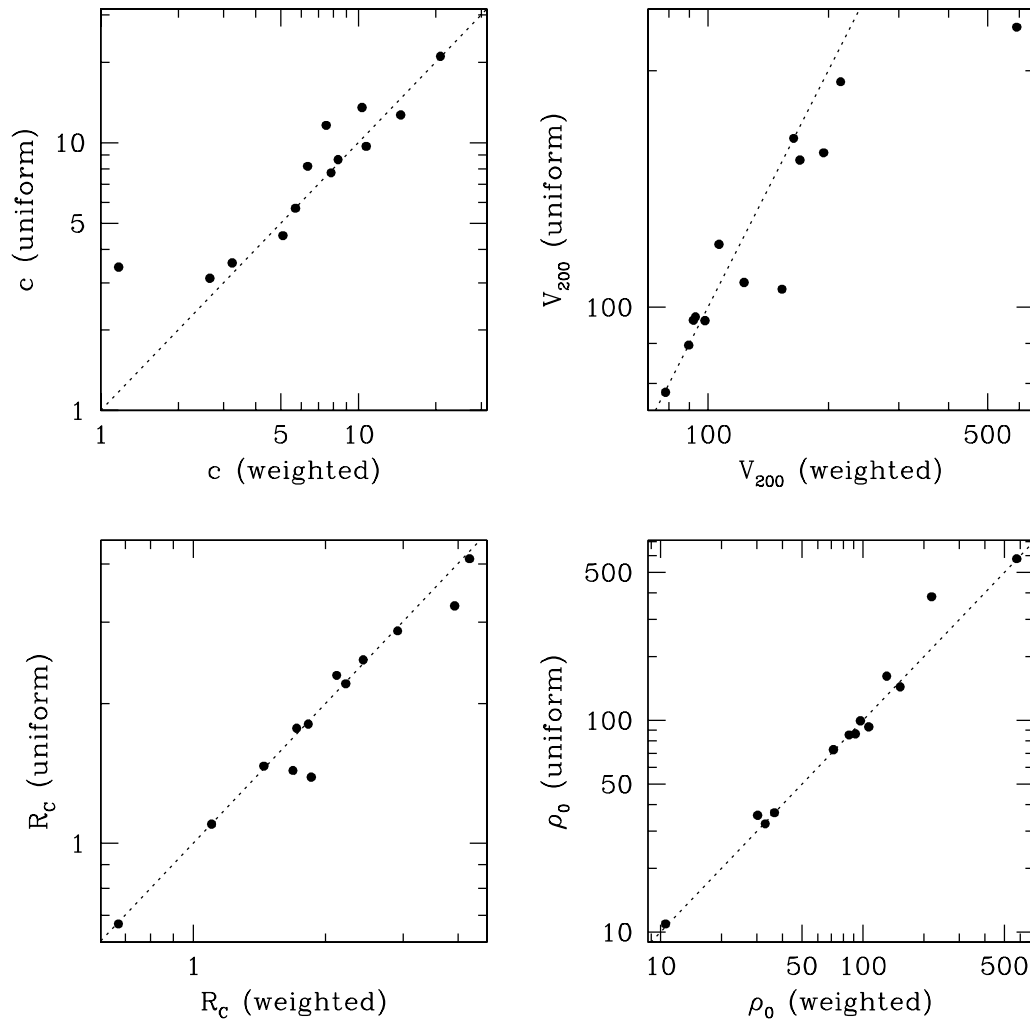
FIG. 5.—Comparison of the NFW halo parameters c and V_{200} and the pseudoisothermal halo parameters R_C and ρ_0, as derived using a weighted model fit, using the inverse variance as weight, and uniform error bars. There is good agreement. The somewhat increased scatter at extreme values is not significant, as the shape of the model in that area of parameter space is fairly insensitive to the precise values.

agreement (see Paper I). This curve is difficult to model with a standard NFW profile, but the pseudoisothermal model provides a good fit. The outermost point is taken from the H I curve and provides an important constraint for the NFW model. Without this point the fit produces $c \sim 0$ and

an impossibly large V_{200}, a result of the fitting program's trying to make $V(R) \sim R^{1/2}$ look like $V \sim R$.

UGC 6614: This is the only giant LSB galaxy in sample I. The analysis is complicated by the presence of a dominant bulge, which we have modeled as an exponential spherical
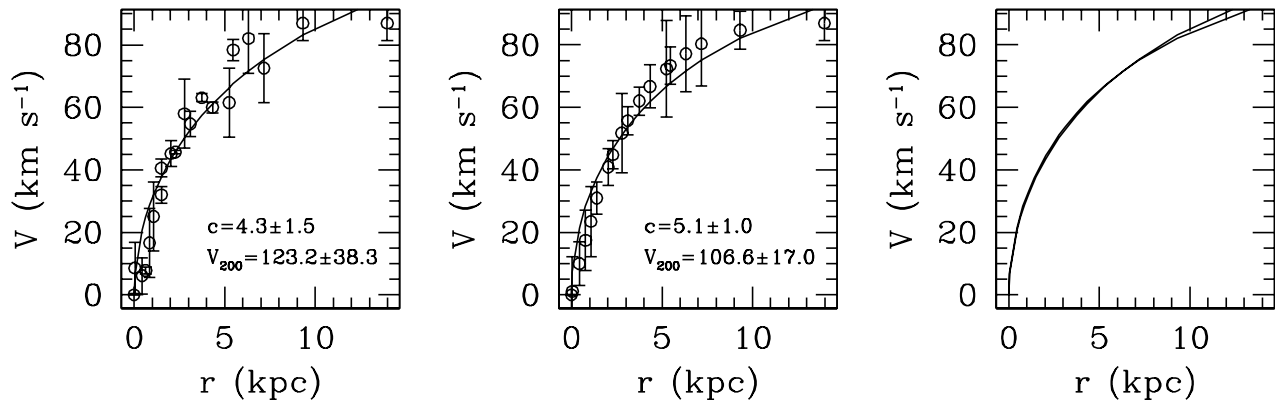

FIG. 6.—Comparison of NFW minimum disk fits to the raw rotation curve of F583-1 (*left*) and the smooth curve (*middle*). The right panel compares the two fits, which are virtually identical. The fit parameters shown in the panels agree within their errors.
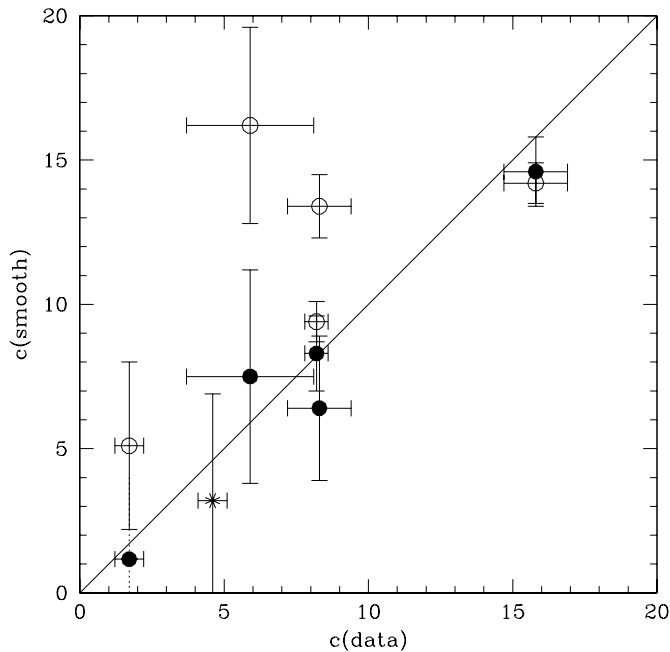
FIG. 7.—Comparison of the NFW halo parameters c fitted to the SMT data. The horizontal axis represents c-values derived from the raw data, the vertical axis those derived from the smooth curves. The open symbols compare the values derived from the raw data with those derived from the SMT smooth curves. The filled symbols compare the raw data results with the values derived from our smooth curves. The star represents the result from our analysis of our data for F568-3. The dotted line in the lower left corner indicates that no realistic error bars could be derived for this fit. Our analysis of the raw, unsmoothed data, of our smoothed versions of these curves, and of the SMT smooth curves shows good agreement. The only exceptions are F563-V2 and F568-1, for which the SMT curves give larger concentrations. While the formal fits differ significantly in these cases, the differences in the curves being fitted are subtle (see Fig. 2). This illustrates the importance of high-accuracy data.

bulge with $h = 3''.0$ and $\mu_0(R) = 18.4$ mag arcsec^{-2}. The disk has parameters $h = 19''$ and $\mu_0(R) = 21.3$ mag arcsec^{-2}. The rapid rise and subsequent dip in the rotation velocity at small radii clearly suggest the dominance of the bulge in this giant LSB galaxy. We have assumed the bulge to be maximal at $\Upsilon_*(R) = 3.7$. As the bulge accounts for most of the rotation velocity in the inner parts, this seems to argue against cuspy halos in giant LSB galaxies.

5. DISCUSSION

5.1. NFW and Pseudoisothermal: A Comparison

The pseudoisothermal halos generally provide better fits than the NFW halos. In Figure 8, we compare the reduced χ^2 values for the four different Υ_* cases. For the minimum disk case we plot samples I and II; for the other cases only sample I is plotted. It is clear that the large majority of the curves presented here are best fitted by a pseudoisothermal halo. This holds true even in the maximum disk case, where one might naively expect the dominance of the optical disk to wipe out any discrepancies of a particular halo model (though perhaps not for LSB galaxies).

Another way of comparing the models is given in Table 9. This lists the number of galaxies in sample I that have good ($p > 0.95$) or bad ($p < 0.05$) fits for each of the two models. Here again it is clear that the pseudoisothermal model performs much better, for every assumption of Υ_*. These statements do not depend on the errors. If we double (or halve)

TABLE 9
COMPARISON PROBABILITIES: NFW VERSUS PSEUDOISOTHERMAL, SAMPLE I

Υ_*	PSEUDOISOTHERMAL HALO		NFW HALO	
	$p > 0.95$	$p < 0.05$	$p > 0.95$	$p < 0.05$
Minimum	8	1	4	3
Min. + gas	8	1	4	4
Constant	10	1	4	4
Maximum	8	3	6	3

NOTE.—Listed is the number of galaxies (out of 13); p is the probability that the model is compatible with the data.

the size of the error bars, χ^2 will change for both halo cases, but it will always remain less for the pseudoisothermal case. To alter this result would require systematic changes to the shapes of all the rotation curves.

Figure 9 shows the residuals of the best-fitting minimum disk models versus the observed data. Residuals are plotted against halo scale size (R_{200} for NFW and R_C for pseudoisothermal halos), radius in kiloparsecs, number of optical disk scale lengths, and fraction of maximum radius of the rotation curve. As described in the previous section, the NFW fits that fail do so in a systematic way: the inner velocity is overestimated, then the model drops below the observed velocities in the middle, and in the outer parts it once again overpredicts the velocity. The NFW residuals are most pronounced when plotted against R/R_{max}. The majority of the residuals change sign at $\sim 0.2R_{max}$ and $\sim 0.7R_{max}$. As the radius R_{max} does not have any physical significance but is determined by the observations (slit angle, presence of Hα, etc.), this indicates that the systematics is due to the choice of model, rather than being associated with any particular length scale in the galaxies. Similar conclusions are reached when the residuals are plotted for the minimum disk plus gas, constant-Υ_*, and maximum disk cases.

Though not readily apparent in Figure 3, the residuals for the pseudoisothermal halo model also show a systematic behavior, though at a much lower level than the NFW model. Here the residuals do not increase toward the center, and as the typical size of the residuals is smaller than the uncertainty in the individual data points, this just shows us that the rotation-curve shape is subtly different from that of a pure pseudoisothermal halo. This should come as no surprise given the simplifying assumptions, for example, minimum disk, that we have made.

5.2. The Pseudoisothermal Halo

Of the two models investigated, the pseudoisothermal halo best describes the data. Here we briefly explore some correlations between the pseudoisothermal halo model parameters and the parameters describing the luminous components of the galaxies. To increase the range of the parameters, we also consider the samples of Broeils (1992) of (mainly) luminous HSB galaxies and Swaters (1999) of late-type dwarf galaxies. From these samples we only select bulgeless galaxies brighter than $M_B = -16.5$, to be consistent with the range of luminosities found in our sample.

Figure 10 presents the results for the three samples. We show the minimum disk plus gas case, which the two comparison samples refer to as their "minimum disk." The most obvious correlation visible in Figure 10 is that between R_C and ρ_0. This is a reflection of the fact that these two are
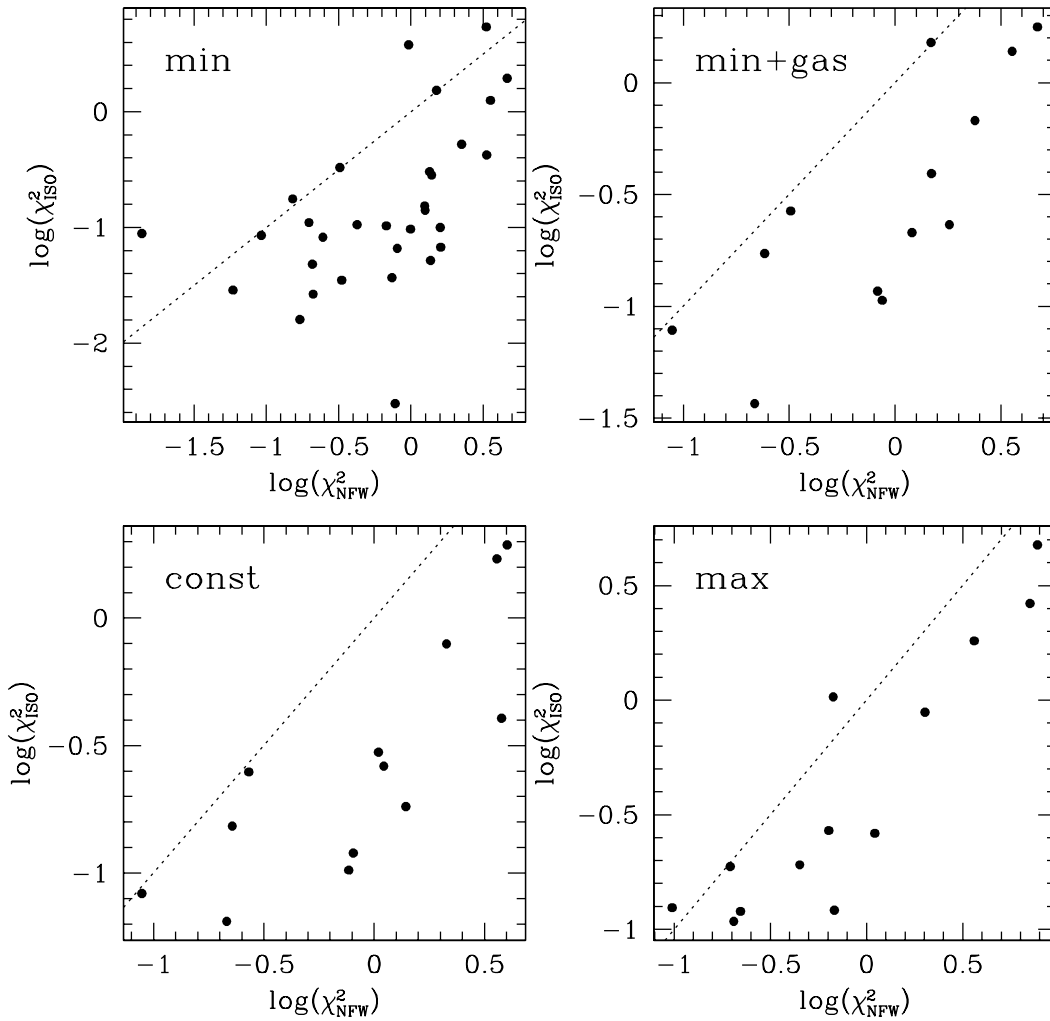
FIG. 8.—Comparison of the reduced χ^2 values using NFW and pseudoisothermal halos, using the four assumptions for Υ_* as described in the text. Note that the axes have logarithmic scales. The dotted lines are lines of equality.

correlated through the asymptotic velocity V_∞ (see eq. [3]). Lines of constant V_∞ have a slope of $-\frac{1}{2}$ in the R_C-ρ_0 diagram, and the diagram therefore just reflects the limited range in V_{max} in the samples. There is an indication that R_C increases toward lower surface brightnesses, and that ρ_0 decreases (as one would expect if LSB galaxies inhabited lower density halos).

The large scatter in these figures sheds little light on galaxy formation or the details of pseudoisothermal halos. How the observed regularities of galaxy kinematics (such as the T-F relation) can emerge from this scatter remains a mystery.

A further analysis is presented in de Blok et al. (2001), where the mass-density distributions that give rise to the observed rotation curves are presented. They show that the minimum disk mass-density distributions at small radii can be parameterized by a power law $\rho \sim r^\alpha$, where for the LSB galaxies $\alpha = -0.2 \pm 0.2$, clearly different from $-1.5 \leq \alpha \leq -1$ as predicted by CDM. These minimum disk slopes are upper limits. When stars are properly taken into account, assuming some reasonable value for Υ_*, the slopes decrease and become even more consistent with constant-density cores. Successful theories of galaxy formation and evolution that attempt to model LSB galaxies

should thus be able to produce halos dominated by constant-density cores.

5.3. The NFW Halo

As noted earlier, the halo parameters c and V_{200} are related. Here we compare the derived c and V_{200} values with those predicted by ΛCDM with the Navarro et al. (1997) prescription for $\Omega_m = 0.3$, $\Omega_\Lambda = 0.7$, and $h = 0.65$ with a COBE-normalized power spectrum. The values of c depend on the assumed Υ_*, which, as discussed before, is uncertain. Minimum disk however gives strong upper limits on the values of c: when Υ_* is increased, the halo needs to compensate by becoming less concentrated (Navarro et al. 1997). Minimum disk models with c-values higher than found in simulations can usually be reconciled with these observations by increasing Υ_* or introducing a bulge to bring the c-values down, as one can see from the progressive decrease in c-values from minimum disk to maximum disk.

Explaining minimum disk models with concentrations lower than the simulated values is more difficult. It indicates one or more of three problems: failure of the model, failure of the assumption of circular motion in deriving rotation curves, or a dramatic (noncosmological) redistribution of dark matter. This last option is not really understood and
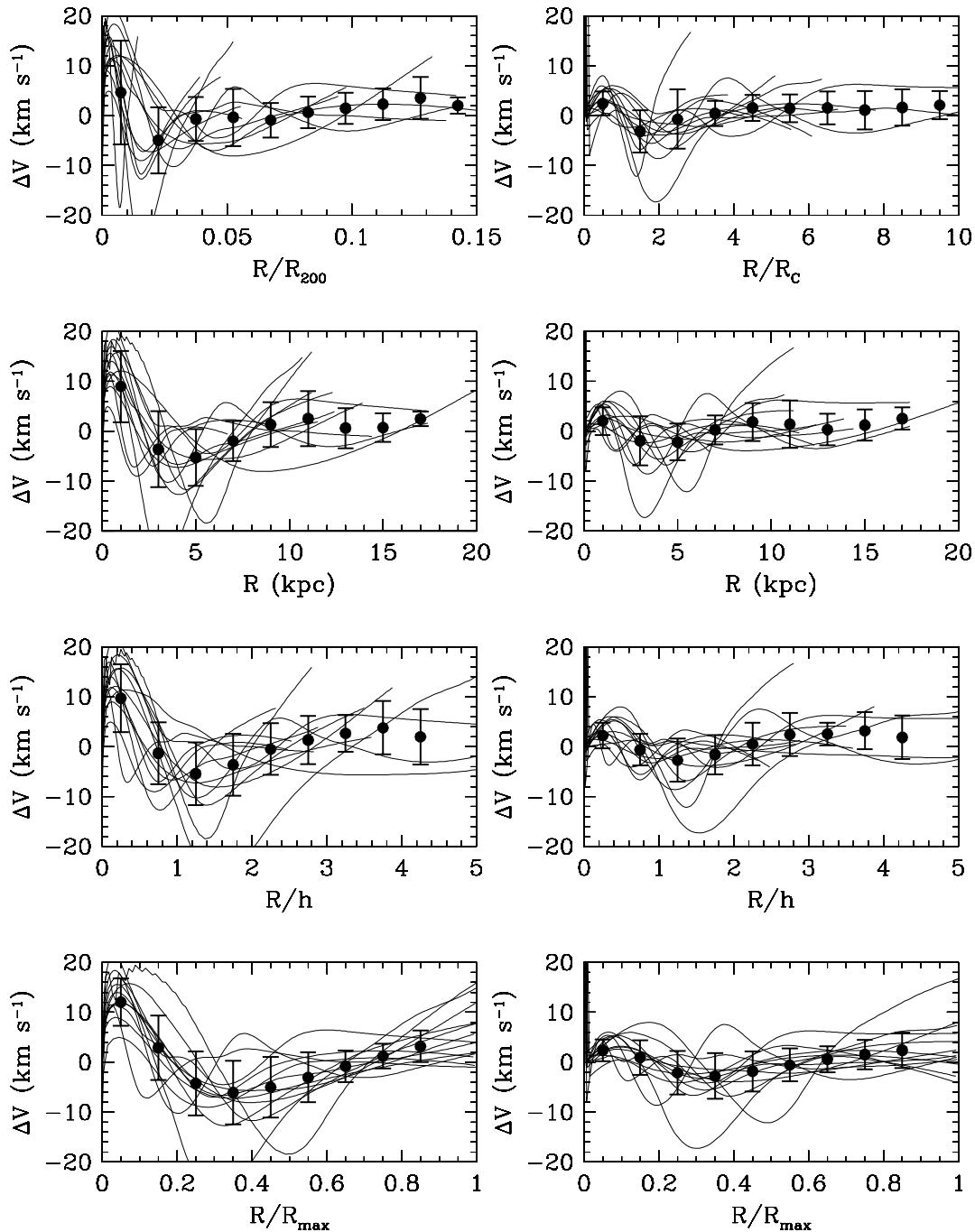
FIG. 9.—Comparison of the residuals $\Delta V = V_{model} - V_{obs}$ for sample I (minimum disk), plotted against number of halo scale radii (*first row*), absolute radius (*second row*), number of optical disk scale lengths (*third row*), and fraction of maximum radius of rotation curve (*fourth row*). The left panels show residuals using NFW halo models, and the right panels show the pseudoisothermal halo case. Also shown are the average residuals and standard deviations (*circles*). The residuals at small radii are much larger for the NFW model than for the pseudoisothermal model. The low-level systematic residuals that are also apparent for the pseudoisothermal halo probably tell us that real halos are subtly different from pseudoisothermal.

potentially removes any of the predictive power that the CDM theory has. We will not discuss it here, except to note that the most plausible effect, adiabatic contraction, further concentrates the dark matter, making the problem worse.

As an aside, we note here that the minimum disk plus gas case sometimes gives slightly higher c-values than the simple minimum disk case. In most cases this is due to a central depression in the H I surface density that gives rise to imaginary rotation velocities, which have to be compen-

sated for by the halo. Also, some of the outer rotation velocity is explained by the gas rotation curve, yielding a halo curve that bends more at small radii. Consequently, the halo model tends to be slightly more concentrated.

Figure 11 shows the derived c and V_{200} values and compares them with the ΛCDM predictions. For the minimum disk case we show both samples I and II; for the other three Υ_*-values only sample I is shown. The data points are coded to indicate their significance level p.
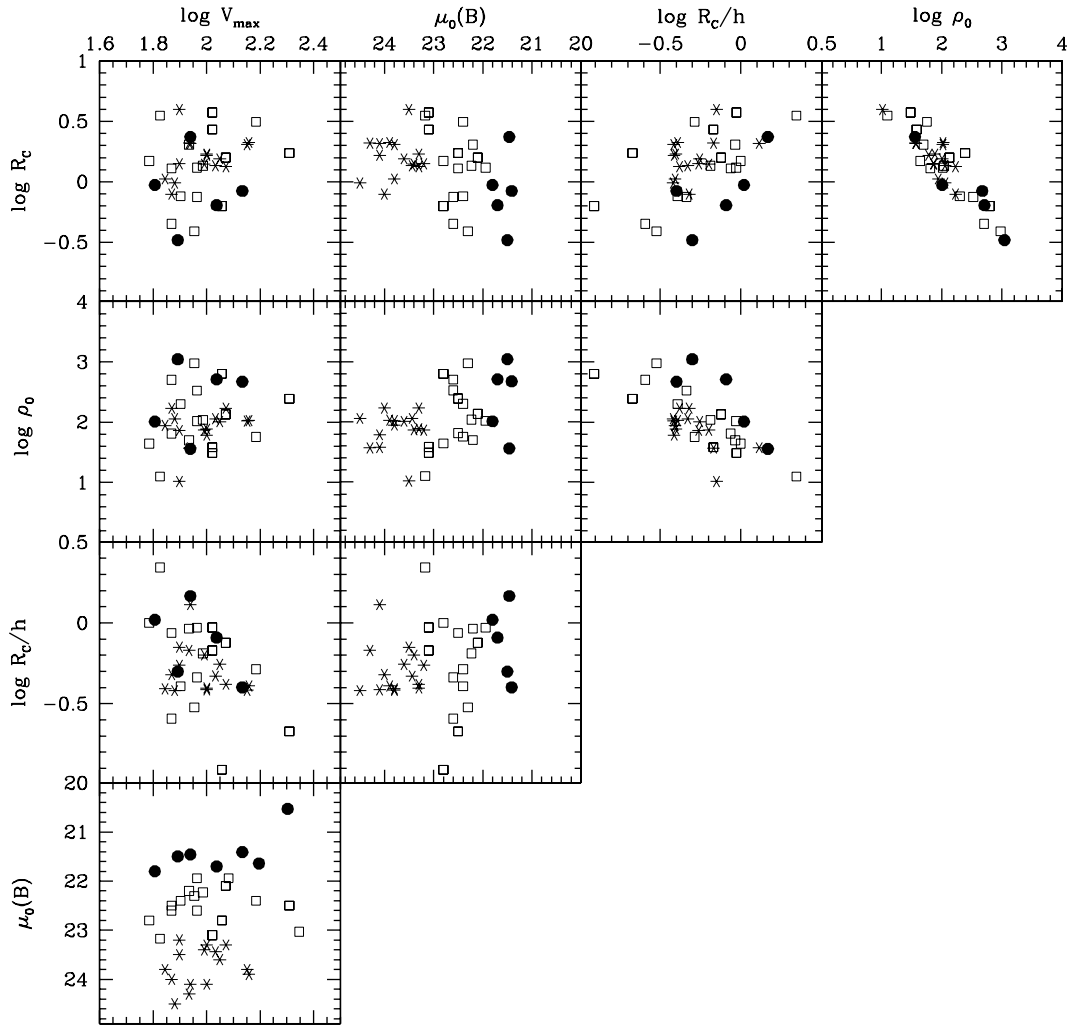
FIG. 10.—Correlations involving pseudoisothermal halo parameters assuming minimum disk plus gas. Shown are maximum rotation velocity V_{max} (km s^{-1}), surface brightness μ_0 (B mag arcsec^{-2}), central halo density ρ_0 (10^{-3} $M_\odot$ pc^{-3}), halo core radius R_C (kpc), and the ratio of core radius and optical disk scale length R_C/h. Included are the bulgeless HSB galaxies brighter than $M_B = -16.5$ from Broeils (1992) and the high-quality ($q = 0$ or $q = 1$) curves of bright $M_B < -16.5$ dwarfs from Swaters (1999). Circles, $\mu_0(B) < 21.9$ mag arcsec^{-2}; squares, $21.9 \leq \mu_0(B) \leq 23.2$; stars, $\mu_0(B) > 23.2$. See text for details.

Several points can be made about Figure 11. First, the bottom right panel clearly shows that maximum disk is inconsistent with the NFW halos expected to arise in ΛCDM. Secondly, there is some correlation between the significance of the fits and their position in the c-V_{200} diagram. In the minimum disk case, the majority (11 out of 14) of the $p > 0.95$ points are found at $V_{200} \lesssim 100$ km s^{-1}. Most (17 out of 19) of the $p < 0.95$ points are found to the right of this line. This division becomes more clear in the minimum disk plus gas and constant-Υ_* plots. As the high V_{200} values tend to occur at lower c, this is likely to be the effect of an NFW halo trying to fit a solid-body–like curve, by hiding its curvature outside the visible galaxy, i.e., by decreasing c and increasing V_{200}.

Thirdly, the distribution of points does not agree with that predicted by the numerical models (Jing 2000; Bullock et al. 2001). There are more points above, but more importantly, below, the 1 σ lines than expected. This low-c tail consists of fits that have a high to reasonable significance p associated with them. We show the distribution again in Figure 12. The two histograms are for minimum disk (*open histogram*; samples I and II) and constant Υ_* (*shaded histo-*

gram; sample I). Overplotted are lognormal distributions showing the distribution derived from numerical simulations. Unfortunately, these simulations do not agree on the value of the dispersion. The ΛCDM model by Bullock et al. (2001) gives a logarithmic dispersion $\sigma_c \simeq 0.18$, while the distribution for relaxed ΛCDM halos as found by Jing (2000) has a logarithmic dispersion of $\sigma_c \simeq 0.08$. The observed distribution is clearly wider than either theoretical one. By changing the cosmology of the model one can change the mean of the distribution (e.g., OCDM has a mean $\log c = 1.25$; Jing 2000), but the width hardly changes. Thus one can possibly shift the model to higher c to fit the high-c end of the distribution, but it is impossible to explain the large observed low-c tail with the kind of lognormal distribution one derives from the simulations.

5.4. Morphology

Rotation curves have the implicit assumption of circular motion. Can noncircular motions affect the rotation curves? As the NFW models show the largest residuals in the centers of some of the LSB galaxies, it is possible that they could be affected by noncircular motions due to non-
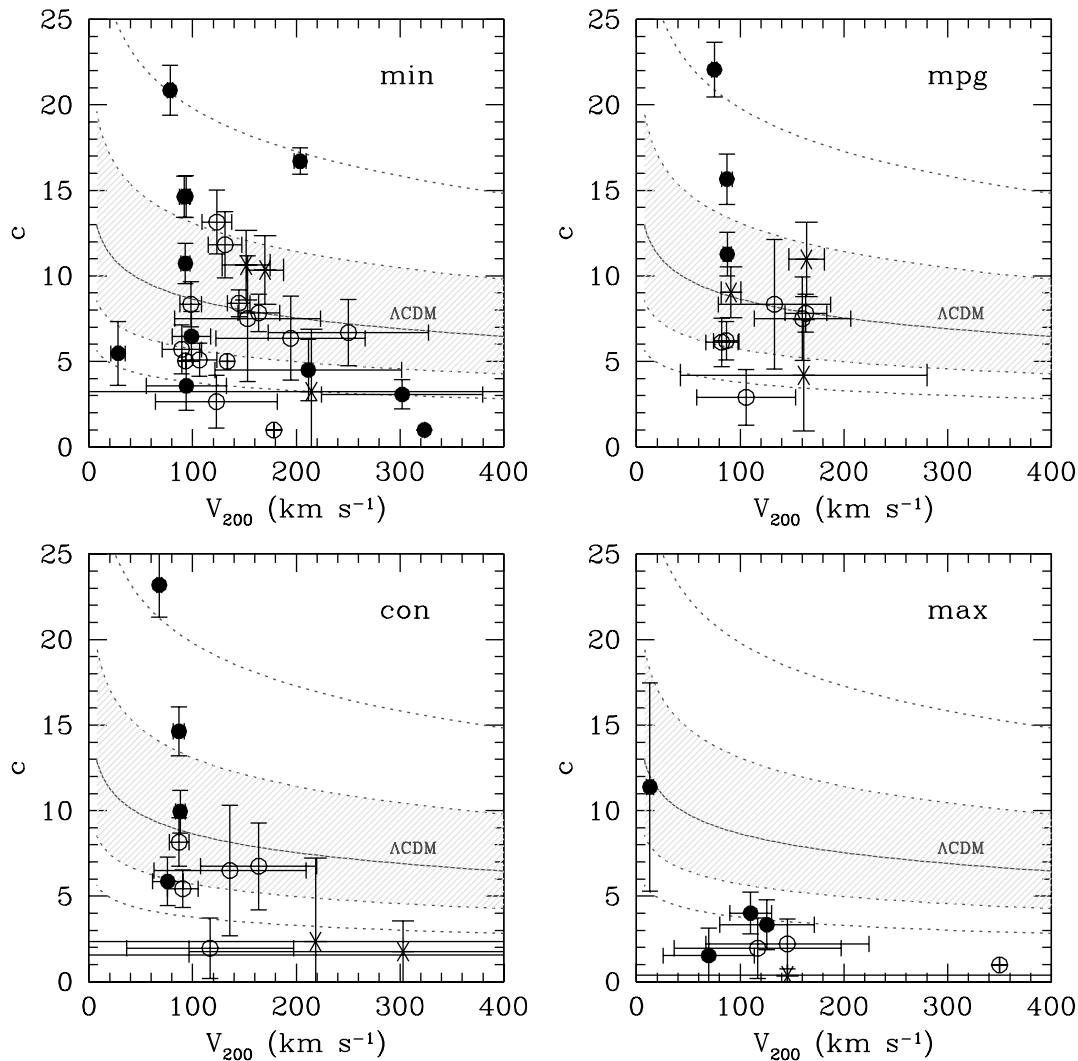
Fig. 11.—NFW halo concentration parameter c plotted against the halo rotation velocity V_{200} for the four different Υ_* cases discussed in this paper. Filled circles represent good fits ($p > 0.95$), open circles average-quality fits ($0.05 < p < 0.95$). Crosses represent bad fits ($p < 0.05$). Good fits are primarily found at $V_{200} < 100$ km s^{-1}. Maximum disk is clearly inconsistent with NFW. The line labeled "ΛCDM" shows the prediction for that cosmology derived from numerical models. The gray area encloses the 1 σ uncertainty (Bullock et al. 2001). The upper and lower dotted lines show the 2 σ uncertainty. The minimum disk panel shows both samples I and II. The other three panels only show sample I.

axisymmetric components. We will investigate the matter here by comparing the morphology of our galaxies with the quality of the fits.

Table 10 contains a short description of the morphology of the galaxies, where we have focused on the central parts. In the table, "core" refers to a galaxy whose central light distribution can best be described by an axisymmetric model, presumably implying negligible noncircular motions in the inner part. The word "core" is used very loosely here. It does not necessarily indicate the presence of a bulge or massive central component but is just an indication of the (deprojected) round shape of the isophotes in the inner part of the galaxy. "Bar" indicates a central morphology dominated by a barlike structure, usually Magellanic, that may indicate the presence of noncircular motions.

The results are summarized in Table 11 (for the minimum disk assumption). The conclusion is that there is no clear dependence of residual velocity on morphology. There is thus no indication that the failure of NFW to fit some

galaxy rotation curves can be attributed to the presence of bars or noncircular motions.

6. THE MAXIMUM DISK

As noted in § 1, the inner rotation curves of HSB galaxies can usually be well explained by scaling up the rotation curve derived from the light distribution. This maximum disk procedure results in Υ_*-values that are reasonably consistent with those derived from stellar population synthesis models (Verheijen 1997; Palunas & Williams 2000; van Albada & Sancisi 1986). Furthermore, bars seem to demand near-maximal disks in HSB galaxies (Debattista & Sellwood 2000; Weiner, Sellwood, & Williams 2001)

The matter of maximum disk in LSB galaxies was first discussed in de Blok & McGaugh (1997), where it was noted that from a stellar population point of view, maximum disk demanded unreasonably high Υ_*-values. Substantial amounts of dark matter were still needed within the optical
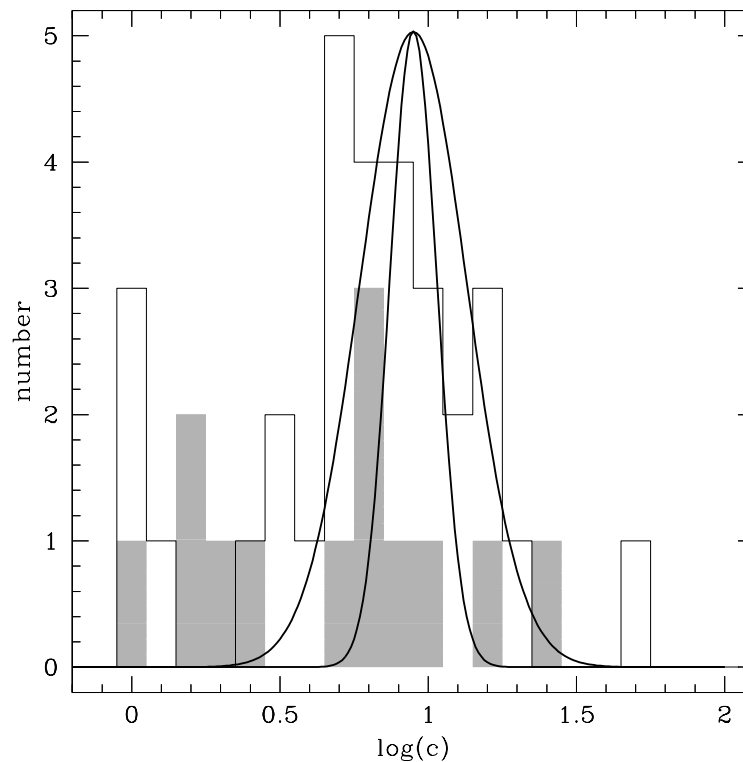
FIG. 12.—Distribution of the c-parameter for the minimum disk case (*open histogram*) and the constant-Υ_* case (*shaded histogram*). Overplotted is the theoretical lognormal distribution for a ΛCDM cosmology, derived from independent numerical simulations by Jing (2000) and Bullock et al. (2001). The former finds a lognormal distribution with a logarithmic dispersion $\sigma_c = 0.08$. The latter finds a wider lognormal distribution with $\sigma_c = 0.18$. The observed low-c tail is not consistent with either theoretical distribution. The theoretical distributions have been arbitrarily normalized to coincide with the maximum of the observed distribution.

disk to explain the observed H I curves. SMT revisited the subject and noted that the slightly steeper slopes they found using their Hα curves enabled them to scale up the disk rotation curve by an even larger factor. The maximum disk Υ_*-value is extremely sensitive to the inner slope, and only a very small increase is needed to change it by a significant factor. In LSB galaxies, the maximum disk Υ_*-values are thus much larger than expected on the basis of colors, metallicities, and star formation histories. The higher Υ_*-values as found by SMT worsened this problem (a consequence already noted in de Blok & McGaugh 1997), despite the fact that their maximum disk models could slightly better reproduce the observed inner curve.

Though it seems unlikely that the maximum disk results can be explained using "reasonable" stellar populations, given what we know about the star formation history, dust content, and metallicity of LSB galaxies, the matter is still relevant for exploring possible baryonic disk dark matter scenarios. To explain maximum disk in LSB galaxies purely in terms of baryons, one has to assume a large amount of unseen material in the form of, for example, cold molecular gas, optically thick neutral hydrogen, or low-mass stars, or due to nonstandard IMFs. It should be noted, though, that many of these hypothetical mass components would violate constraints imposed by disk stability (Athanassoula, Bosma, & Papaioannou 1987; Mihos, McGaugh, & de Blok 1997) and near-IR colors (Bell et al. 2000; Bell & de Jong 2000) and could possibly introduce a surface brightness segregation in the baryonic T-F relation (McGaugh et al. 2000)

In Figure 13, we compare the maximum disk B-band Υ_*

ratios[2] for sample I with those derived by Broeils (1992) for a sample of mostly HSB galaxies and by Swaters (1999) for a sample of dwarfs. We again show only bulgeless galaxies brighter than $M_B = -16.5$. Also indicated are Υ_*-values from Bell & de Jong (2001), who tabulate stellar mass-to-light ratios for various star formation histories and population synthesis models as a function of color. Here we show representative values (assuming a simple Salpeter IMF) spanning the color range exhibited by late-type HSB galaxies, gas-rich dwarfs, and LSB galaxies.

The Υ_*-values for HSB galaxies agree to within a factor of 3 and can be considered to be (close to) maximum disk. The values found for LSB galaxies and dwarfs are less easily reconciled with the model values. Observationally, values up to $\Upsilon_*(B) = 15$ are found, while the typical model value (again for a simple Salpeter IMF) is $\Upsilon_*(B) \simeq 0.9$ for $B-R = 0.8$ (the average color for a dwarf/LSB galaxy). This discrepancy cannot be explained with extinction or population effects. Extinction in dwarfs and LSB galaxies is less than in HSB galaxies (Tully & Verheijen 1998), and a factor of ~ 17 (3.0 mag) extinction is hard to reconcile with the known properties of LSB galaxies. Line-of-sight extinctions observed toward H II regions in LSB galaxies are never as large (McGaugh 1994; de Blok & van der Hulst 1998).

---

[2] These were derived by converting our R-band values using the $B-R$ color. We converted our data to B band, rather than converting the HSB data to R band, as the colors of LSB galaxies are better determined than those of the Broeils HSB galaxies. The color gradients in LSB galaxies are small, so systematic effects are negligible.

TABLE 10
MORPHOLOGY AND PROBABILITY: NFW HALOS

Galaxy	Prob.[a]	Core[b]	Bar[b]	Morphology
F563-1	+	−	+	Magellanic irregular
F563-V2	0	−	+	Magellanic bar
F568-1	0	+	−	Spiral
F568-3	−	−	+	Spiral with Magellanic bar
F568-V1	+	+	−	Spiral
F571-8	0	+	?	Edge-on
F574-1	−	+	−	Disk
F579-V1	+	+	−	Core, flocculent arms
F583-1	0	+	−	Magellanic irregular
F583-4	+	+ ?	+ ?	Fuzzy
F730-V1	0	+	−	Spiral
UGC 4115	0	+ ?	−	Fuzzy
UGC 5750	0	−	+	Magellanic bar
UGC 6614	−	+	−	Faint, with bulge
UGC 11454	−	+	−	Fuzzy spiral, small core
UGC 11557	0	+	−	Fuzzy spiral, small core
UGC 11583	0	−	+	Faint Magellanic bar
UGC 11616	0	+	−	Fuzzy, irregular
UGC 11648	0	−	+	Irregular
UGC 11748	−	+	+ ?	Irregular, bright core/bar?
UGC 11819	0	+	−	Fuzzy
ESO-LV 014-0040......	+	+	−	Spiral
ESO-LV 084-0411......	−	−	?	Edge-on
ESO-LV 120-0211......	+	−	+	Fuzzy Magellanic bar
ESO-LV 187-0510......	+	−	+	Irregular spiral, flocculent
ESO-LV 206-0140......	+	+	−	Spiral
ESO-LV 302-0120......	+	+	+ ?	Spiral, hint of bar?
ESO-LV 305-0090......	+	+	+	Barred spiral
ESO-LV 425-0180......	+	+	−	Spiral
ESO-LV 488-0490......	+	−	+	Inclined Magellanic bar

[a] Here " + " indicates a good fit, $p \geq 0.95$; "0" indicates an average fit, $0.05 < p < 0.95$; " − " indicates a bad fit, $p < 0.05$.

[b] Here " + " indicates that the component is clearly present; " − " indicates that it is not obviously present.

Apart from changing the IMF in an ad hoc way, it is hard to see how such high Υ_*-values can be reached given the constraints imposed by what we know about the star formation history (low star formation rate in the past and at present) and the blue (optical and near-IR) colors of LSB galaxies (de Blok et al. 1995; McGaugh & Bothun 1994; van den Hoek et al. 2000; Bell et al. 2000; Bell & de Jong 2000; de Jong 1996). It is likely that the maximum disk values as found in LSB galaxies are not representative of the evolutionary stage of these galaxies. While the maximum disk prescription now has somewhat greater success in predicting the inner shape of the rotation curves of LSB galaxies, it requires stellar mass-to-light ratios that are too large for the stellar populations in these galaxies. The mass discrepancies are still large; all this does is move the dark matter from halo to disk.

TABLE 11
MORPHOLOGY AND PROBABILITY SUMMARY: NFW HALOS

Quality	Bar	Core	Both
Good ($p > 0.95$)	4	7	3
Bad ($p < 0.05$)	2	4	0
Unclear ($0.05 < p < 0.95$)......	4	7	1

NOTE.—Listed value indicates the number of minimum disk fits of that quality in presence of the component mentioned.

6.1. Maximum Surface Density of a Disk

Just as the minimum disk assumption gives us an upper limit on the amount of dark matter implied by rotation curves, the maximum disk hypothesis gives us an upper limit on the amount of mass that could potentially be hidden in a disk. It is therefore still useful to ask ourselves what these maximum disk upper limits imply for the stellar disks.

Maximum disk means maximum surface density (luminous surface density times Υ_*) and therefore gives an absolute upper limit on the mass surface density in stellar disks (for mass components that are distributed like the stars). Figure 14 summarizes the maximum disk results for the sample I LSB galaxies, as well as the Broeils (1992) and Swaters (1999) HSB and dwarf samples. We plot the maximum disk Υ_*-values, as well as the luminosity, rotation velocity, surface brightness, and maximum disk surface density. The data are divided into three surface brightness bins. As already shown in de Blok & McGaugh (1997), at fixed V_{max} LSB galaxies have higher maximum Υ_*-values than HSB galaxies.

Figure 14 also shows the maximum surface density σ. As the decrease in surface brightness is faster than the increase in maximum disk Υ_*, toward low surface brightnesses the maximum surface density σ in a disk decreases with surface brightness. The μ_0-σ panel suggests that there is a well-defined upper limit to the maximum surface density that
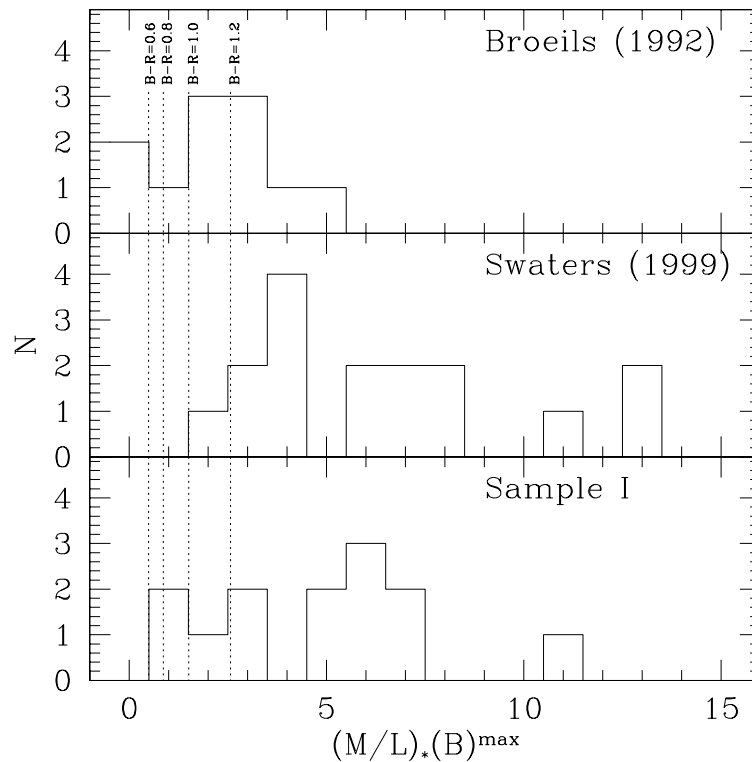
FIG. 13.—Histograms of the maximum disk Υ_*-values. The top panel refers to bulgeless galaxies from the collection of Broeils (1992) brighter than $M_B = -16.5$. The middle panel refers to dwarf galaxies brighter than $M_B = -16.5$ from Swaters (1999) with quality index 0 or 1 (very good to good). The bottom panel shows sample I. Also indicated are the values for Υ_* using population synthesis models by Bell & de Jong (2001) assuming a simple Salpeter IMF.

disks can attain. Even under maximum disk, LSB galaxy disks have, on average, lower surface densities than HSB galaxy disks, again putting limits on the amount of baryonic mass one can hide in these disks.

Figure 3 shows that even in the maximum disk case most LSB galaxies have $V_{max}(disk) < V_{max}(observed)$. Therefore, even in the maximum disk case a moderate amount of dark matter is still required in the optical disk. It is therefore hard to explain the T-F relation for LSB galaxies in the context of maximum disk: the stellar disk then needs to provide the luminosity *and* the necessary rotation velocity. LSB galaxies would deviate systematically from the HSB T-F relation, which is evidently not the case (Zwaan et al. 1995).

This is illustrated in the inset panel in Figure 14 (*bottom right*). Using the arguments in Zwaan et al. (1995), we find that $\Sigma_0(\Upsilon)^2$ needs to be constant for galaxies to obey a T-F relation independent of surface brightness. If all galaxies were truly maximum disk [in the sense that $V_{max}(disk) \simeq V_{max}(observed)$], one could replace this by the requirement that $\Sigma_0(\Upsilon_*)^2_{max}$ needs to be constant. The bottom right panel shows that this is not the case: at fixed V_{max}, there is a substantial scatter that would translate into ~ 5 mag scatter in T-F. Clearly the observed scatter is much smaller, and this shows the clear need for an additional mass component to make T-F work. In other words, maximum disk for *all* galaxies and T-F are incompatible.

7. CONCLUSIONS

The most important conclusion from this work is that the large majority of the high-resolution rotation curves presented here prefer the pseudoisothermal core-dominated

halo model. For a small number of galaxies, neither the pseudoisothermal nor the NFW model is an adequate description of the data. This should not come as a surprise, as the true dark matter distribution is likely to be more complex than the models presented here. Nevertheless, the general trend is that for almost all galaxies discussed here the relative quality of the fits using the pseudoisothermal model is better than those for the NFW model.

For a small number of galaxies the NFW model provides a good fit, but generally the concentrations derived from the observed rotation curves are lower than predicted by the simulations. This is hard to fix: the most likely effect that may alter the initial cosmological NFW halo is adiabatic contraction, but this has the effect of making the final (observed) halo *more* concentrated, so one would have to start off with (cosmologically relevant) halos that are even *less* concentrated.

It is worrying that for one or two extreme cases the difference between "CDM does work" or "CDM does not work" depends on subtle differences in data, data handling, or analysis. Figure 7 illustrates that opposite claims can sometimes be made from the same data. Hence we reiterate the need for the highest quality data of a large sample, in order to minimize these effects.

We refer to de Blok et al. (2001), where it is shown that *all* data presented here are consistent with a core-dominated model; the good NFW fits that are found for a number of LSB galaxies can be attributed to resolution effects.

We summarize our results as follows:

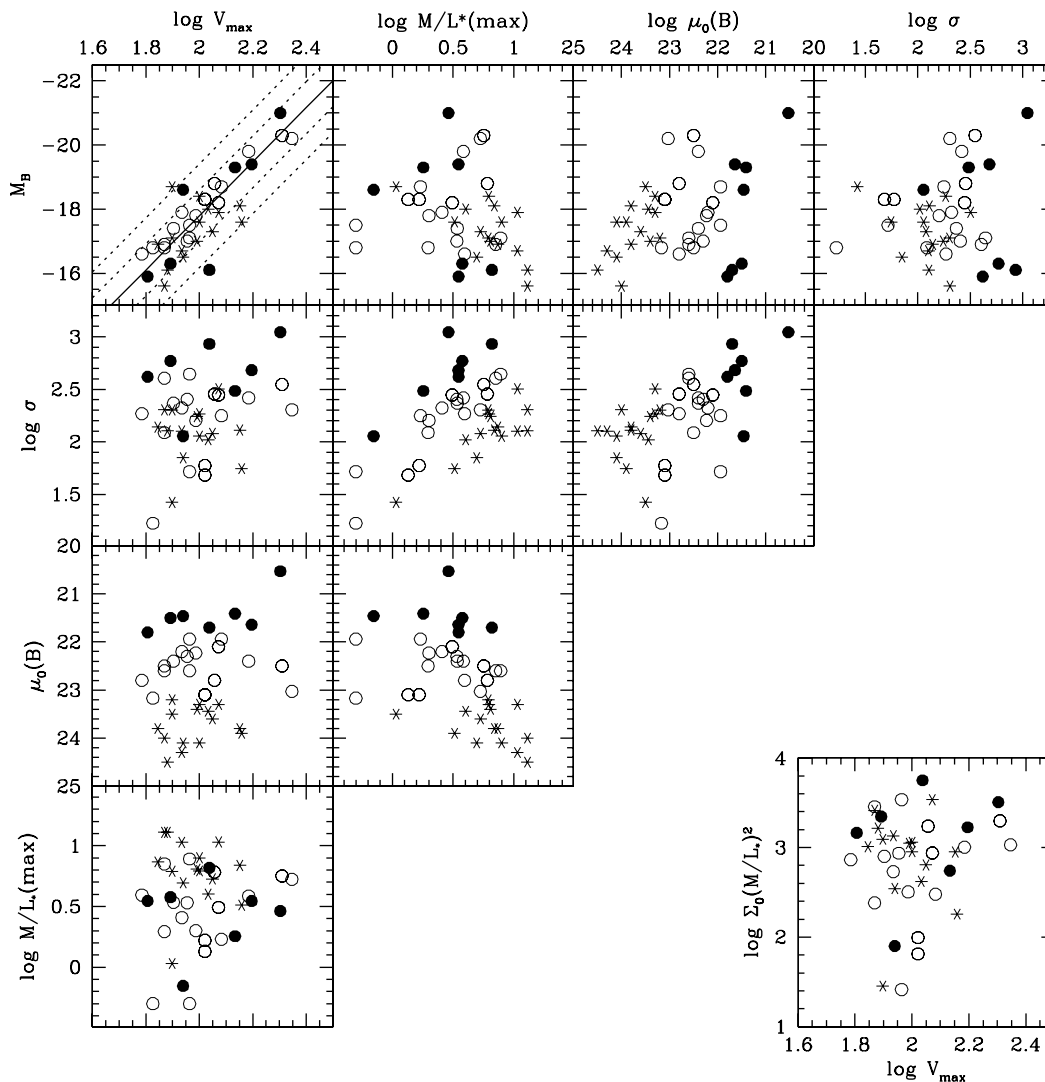1. Pseudoisothermal halos are a better description of the data than NFW halos.

FIG. 14.—Correlations between maximum disk surface density σ ($M_\odot$ pc^{-2}), surface brightness μ_0 (B mag arcsec^{-2}), maximum disk $\Upsilon_*(B)$ [$(M/L_B)_\odot$], maximum observed rotation velocity V_{max} (km s^{-1}), and luminosity M_B (mag). Included again are the bulgeless bright HSB galaxies from Broeils (1992) and the high-quality curves of bright dwarfs from Swaters (1999), as described in the previous figure legend. Filled circles, $\mu_0(B) < 21.9$ mag arcsec^{-2}; open circles, $21.9 \leq \mu_0(B) \leq 23.2$; stars, $\mu_0(B) > 23.2$. The inset panel in the lower right corner shows the product $\Sigma_0(\Upsilon_*)^2$, where Σ_0 is the central surface brightness expressed in $L_\odot$ pc^{-2}. This product should be constant with small scatter for a maximum disk interpretation of the T-F relation. The T-F relation is shown in the top left corner. It has a slope of -8.4. The dotted lines represent the 1 σ and 2 σ scatter, where $\sigma = 0.81$ mag. This scatter is reduced to 0.51 mag when the four most outlying points are omitted (all galaxies with low inclinations).

2. The number of galaxies that cannot be fitted with NFW halos is significantly larger than the number of galaxies that cannot be fitted with the pseudoisothermal model.

3. The quality of the fit is not obviously related to morphology, luminosity, or surface brightness.

4. A larger number of low-c NFW halos is found than one would expect based on the distribution derived from CDM simulations.

5. If one were to construct models that would have the correct c-V_{200} values as predicted by cosmology, the resulting Υ_*-values would be too low to be consistent with stellar population numbers. The shape of the curves would still be wrong.

6. The maximum disk prescription works to predict the inner rotation-curve shape to some extent but gives mass-to-light ratios that are too high to be accounted for by stellar population synthesis models.

7. Applying the maximum disk values yields absolute upper limits on the disk mass surface density that are strongly correlated with surface brightness.

REFERENCES

Athanassoula, E., Bosma, A., & Papaioannou, S. 1987, A&A, 179, 23
Begeman, K. G. 1987, Ph.D. thesis, Univ. Groningen
Bell, E. F., Barnaby, D., Bower, R. G., de Jong, R. S., Harper, D. A., Hereld, M., Loewenstein, R. F., & Rauscher, B. J. 2000, MNRAS, 312, 470
Bell, E. F., & de Jong, R. S. 2000, MNRAS, 312, 497
———. 2001, ApJ, 550, 212
Blais-Ouellette, S., Amram, P., & Carignan, C. 2001, AJ, 121, 1952
Bosma, A., Byun, Y., Freeman, K. C., & Athanassoula, E. 1992, ApJ, 400, L21
Bothun, G., Impey, C., & McGaugh, S. 1997, PASP, 109, 745
Bottema, R. 1997, A&A, 328, 517
Broeils, A. H. 1992, Ph.D. thesis, Univ. Groningen
Bruzual A., G., & Charlot, S. 1993, ApJ, 405, 538
Bullock, J. S., Kolatt, T. S., Sigad, Y., Somerville, R. S., Kravtsov, A. V., Klypin, A. A., Primack, J. R., & Dekel, A. 2001, MNRAS, 321, 559
Casertano, S. 1983, MNRAS, 203, 735
Cole, S., Lacey, C. G., Baugh, C. M., & Frenk, C. S. 2000, MNRAS, 319, 168
Côté, S., Carignan, C., & Freeman, K. C. 2000, AJ, 120, 3027
Debattista, V. P., & Sellwood, J. A. 2000, ApJ, 543, 704
de Blok, W. J. G., & Bosma, A. 2001, A&A, submitted
de Blok, W. J. G., & McGaugh, S. S. 1996, ApJ, 469, L89
———. 1997, MNRAS, 290, 533
de Blok, W. J. G., McGaugh, S. S., Bosma, A., & Rubin, V. C. 2001, ApJ, 552, L23
de Blok, W. J. G., McGaugh, S. S., & van der Hulst, J. M. 1996, MNRAS, 283, 18 (BMH)
de Blok, W. J. G., & van der Hulst, J. M. 1998, A&A, 335, 421
de Blok, W. J. G., van der Hulst, J. M., & Bothun, G. D. 1995, MNRAS, 274, 235
de Jong, R. S. 1996, A&A, 313, 377
Flores, R. A., & Primack, J. R. 1994, ApJ, 427, L1
Freeman, K. C. 1970, ApJ, 160, 811 (erratum 161, 802)
Jing, Y. P. 2000, ApJ, 535, 30
Lake, G., & Feinswog, L. 1989, AJ, 98, 166
Loader, C. 1999, Local Regression and Likelihood (New York: Springer)

Mac Low, M.-M., & Ferrara, A. 1999, ApJ, 513, 142
Matthews, L. D., & Wood, K. 2001, ApJ, 548, 150
McGaugh, S. S. 1994, ApJ, 426, 135
McGaugh, S. S., & Bothun, G. D. 1994, AJ, 107, 530
McGaugh, S. S., & de Blok, W. J. G. 1997, ApJ, 481, 689
———. 1998, ApJ, 499, 41
McGaugh, S. S., Rubin, V. C., & de Blok, W. J. G. 2001, AJ, 122, 2381 (Paper I)
McGaugh, S. S., Schombert, J. M., Bothun, G. D., & de Blok, W. J. G. 2000, ApJ, 533, L99
Mihos, J. C., McGaugh, S. S., & de Blok, W. J. G. 1997, ApJ, 477, L79
Moore, B. 1994, Nature, 370, 629
Moore, B., Quinn, T., Governato, F., Stadel, J., & Lake, G. 1999, MNRAS, 310, 1147
Navarro, J. F., Frenk, C. S., & White, S. D. M. 1996, ApJ, 462, 563
———. 1997, ApJ, 490, 493
Palunas, P., & Williams, T. B. 2000, AJ, 120, 2884
Salucci, P. 2001, MNRAS, 320, L1
Sprayberry, D., Impey, C. D., Bothun, G. D., & Irwin, M. J. 1995, AJ, 109, 558
Swaters, R. A. 1999, Ph.D. thesis, Univ. Groningen
Swaters, R. A., Madore, B. F., & Trewhella, M. 2000, ApJ, 531, L107 (SMT)
Tully, R. B., & Verheijen, M. A. W. 1997, ApJ, 484, 145
van Albada, T. S., & Sancisi, R. 1986, Philos. Trans. R. Soc. London A, 320, 447
van den Bosch, F. C., Robertson, B. E., Dalcanton, J. J., & de Blok, W. J. G. 2000, AJ, 119, 1579
van den Hoek, L. B., de Blok, W. J. G., van der Hulst, J. M., & de Jong, T. 2000, A&A, 357, 397
van der Hulst, J. M., Skillman, E. D., Smith, T. R., Bothun, G. D., McGaugh, S. S., & de Blok, W. J. G. 1993, AJ, 106, 548
van der Kruit, P. C., & Searle, L. 1981, A&A, 95, 105
Verheijen, M. A. W. 1997, Ph.D. thesis, Univ. Groningen
Weiner, B. J., Sellwood, J. A., & Williams, T. B. 2001, ApJ, 546, 931
Zwaan, M. A., van der Hulst, J. M., de Blok, W. J. G., & McGaugh, S. S. 1995, MNRAS, 273, L35